CrossMark

ARTICLE

Triggers on sulfide saturation in Fe–Ti oxide-bearing, mafic-ultramafic layered intrusions in the Tarim large igneous province, NW China

Jun Cao [1,3] · Christina Yan Wang [2] · Yi-Gang Xu [1] · Chang-Ming Xing [2] · Ming-Hao Ren [1]

Abstract Three Fe–Ti oxide-bearing layered intrusions (Mazaertag, Wajilitag, and Piqiang) in the Tarim large igneous province (NW China) have been investigated for understanding the relationship of sulfide saturation, Platinum-group element (PGE) enrichment, and Fe–Ti oxide accumulation in layered intrusions. These mafic-ultramafic layered intrusions have low PGE concentrations (<0.4 ppb Os, <0.7 ppb Ir, <1 ppb Ru, <0.2 ppb Rh, <5 ppb Pt, and <8 ppb Pd) and elevated Cu/Pd (2.2×10^4 to 3.3×10^6). The low PGE concentrations of the rocks are mainly attributed to PGE-depleted, parental magma that was produced by low degrees of partial melting of the mantle. The least contaminated rocks of the Mazaertag and Wajilitag intrusions have slightly enriched Os isotopic compositions with γ_{Os}(t = 280 Ma) values ranging from +13 to +23, indicating that the primitive magma may have been generated from a convecting mantle, without appreciable input of lithospheric mantle. The Mazaertag and Wajilitag intrusions have near-chondritic γ_{Os}(t) values (+13

to +60) against restricted ε_{Nd}(t) values (−0.4 to +2.8), indicating insignificant crustal contamination. Rocks of the Piqiang intrusion have relatively low ε_{Nd}(t) values of −3.1 to +1.0, consistent with ~15 to 25 % assimilation of the upper crust. The rocks of the Mazaertag and Wajilitag intrusions have positive correlation of PGE and S, pointing to the control of PGE by sulfide. Poor correlation of PGE and S for the Piqiang intrusion is attributed to the involvement of multiple sulfide-stage liquids with different PGE compositions or sulfide-oxide reequilibration on cooling. These three layered intrusions have little potential of reef-type PGE mineralization. Four criteria are summarized in this study to help discriminate between PGE-mineralized and PGE-unmineralized mafic-ultramafic intrusions.

Keywords Fe–Ti oxide-bearing · Mafic-ultramafic layered intrusions · Platinum-group elements · Re–Os isotopes · Sulfide saturation · Plume-lithosphere interaction · Tarim large igneous province

---

✉ Yi-Gang Xu
yigangxu@gig.ac.cn

1 State Key Laboratory of Isotope Geochemistry, Guangzhou Institute of Geochemistry, Chinese Academy of Sciences, Guangzhou 510640, China

2 CAS Key Laboratory of Mineralogy and Metallogeny, Guangzhou Institute of Geochemistry, Chinese Academy of Sciences, Guangzhou 510640, China

3 College of Earth Sciences, East China University of Technology, Nanchang 330013, China

Introduction

Platinum-group element (PGE) mineralization may occur in diverse rock types and at various stratigraphic levels in layered intrusions of any size or age (Maier 2005) (Table 1). Economic PGE-rich reefs or horizons are commonly hosted in less evolved, ultramafic cumulates, and associated with chromitite seams in the lower part of giant layered intrusions such as the Bushveld complex in South Africa (e.g., Buchanan et al. 1981; Naldrett et al. 2009), the Stillwater complex in USA (e.g., Campbell et al. 1983) and the Great Dyke in Zimbabwe (e.g., Wilson and Prendergast 2001), or small ultramafic sills such as the Jinbaoshan intrusion in SW China (Wang et al. 2010). The PGE-rich reefs or horizons of these intrusions usually contain

Table 1 Summary for occurrences and major characteristics of some important PGE-mineralized and PGE-unmineralized layered intrusions in the world

Name	Country/craton	Age (Ma)	Size (km^2)	Thickness (km)	PGE mineralization occurrence	Position of reef	Reef rock type	Parental magma
Bushveld complex[a]	South Africa/Kaapvaal	2060	65000	7–9	UG2 chromitite; LG/MG chromitites	Lower	Cr	SHMB
					Merensky reef	Central	Opx-cr-(hz)	
Stillwater[a]	USA/Wyoming	2700	4400	6.5	J-M reef	Central	Opx	SHMB
Great dike[a]	Zimbabwe	2460	3300	3	MSZ	Lower	Cr	SHMB
Rincon del Tigre[a]	Bolivia/Aguapei mobile belt	99	1600	>3	Precious Metals zone	Upper	Mt-gb	
Skaergaard[a]	East Greenland	55	90	3.5	Platinova reef	Upper	Gb	Basalt
Rio Jacare[a]	Brazil/Sao Francisco	2640	84	1		Upper	Mt	
Hongge[b]	China/Yangtze	259	60	1.2		Lower	Ol-cpx	Ferrobasalt
Panzhihua[c]	China/Yangtze	263	30	2–3	×			Ferrobasalt
Baima[d]	China/Yangtze	262	25	1.6	×			Ferrobasalt
Piqiang	China/Tarim	276	16.7		×			
Wajilitag	China/Tarim	283	12	0.11–0.27	×			
Stella[a]	RSA/Kaapvaal	3034	>10	>1		Upper	Mt-gb	
Sonju Lake[a]	USA/Superior	1096	>10	1.2	Precious Metals zone	Upper	Gb	Tholeiite
Xinjie[e]	China/Yangtze	259	10	1.2	PGE horizon 1-4	Lower	Cpx	Ferropicrite
Munni Munn[a]	Australia/Pilbara	2927	5.5	225	LSZ, Dream Reef	Lower	opx/dun-webst	SHMB
Jinbaoshan[f]	China/Yangtze	259	4.8	0.008–0.17	PGE horizon 1-3	Lower	Wehr	Picrite
Mazaertag	China/Tarim	279	0.13	1	×			

Opx orthopyroxenite, *Cpx* clinopyroxenite, *Cr* chromitite, *Hz* harzburgite, *Gb* gabbro, *Mt-gb* magnetite gabbro, *Ol-cpx* olivine clinopyroxenite, *Dun* dunite, *Webst* websterite, *Wehr* wehrlite, *SHMB* siliceous high magnesium basalt

[a] Maier et al. (2005)

[b] Zhong et al. (2002)

[c] Zhou et al. (2005)

[d] Zhang et al.(2013c); Liu et al. (2014)

[e] Zhong et al. (2011)

[f] Wang et al. (2010)

visible sulfides (0.5–5 %, Naldrett 2004). The high PGE concentrations of the reefs or horizons are attributed to high mass ratio of silicate and sulfide melt (R-factor, Campbell and Naldrett 1979) so that PGE from the large volume of magma can be significantly extracted to the small volume of sulfide melt (Li et al. 2001).

Some PGE-rich layers are also associated with Fe–Ti oxide-bearing gabbro and less commonly pyorxenite in the upper levels of layered intrusions, such as those in the Skaergaard intrusion in Greenland (e.g., Holwell and Keays 2014), the Stella intrusion in South Africa (Maier et al. 2003), the Rincón del Tigre Complex in Bolivia (Prendergast 2000), and the Rio Jacaré intrusion in Brazil (Sa et al. 2005). PGE in these reefs is concentrated in the small amounts of Cu–Fe- and Au–Pd-bearing sulfides which is attributed to a delayed sulfide saturation due to the crystallization of magnetite (Prendergast 2000; Maier et al. 2003; Mungall and Naldrett 2008; Holwell and Keays 2014). In contrast, the Fe–Ti oxide-rich layers in the evolved, upper portions of the layered

intrusions such as the Bushveld Complex are PGE-barren (e.g., Barnes et al. 2004). Therefore, it is enigmatic why PGE reef/horizon is associated with Fe–Ti oxide-rich layers in some layered intrusions, but not in others.

In small layered intrusions such as the Xinjie and Hongge intrusions in the Emeishan large igneous province (LIP) in SW China, thin PGE-rich layers are hosted in ultramafic cumulates but associated with Fe–Ti oxide-rich layers rather than chromitite seams (Zhong et al. 2002, 2011). The PGE-rich layers were considered to be a result of sulfide saturation due to early crystallization of Fe–Ti oxides and mixing of primary and evolved magma (Zhong et al. 2002, 2011). The PGE concentrations of the rocks in these intrusions are much lower than those in the Bushveld Complex and the Stella and Jinbaoshan intrusions. The rocks of the layered intrusions in the Tarim LIP contain even less PGE than those in the Emeishan LIP (Zhang et al. 2014). However, it remains unknown why the rocks in the layered intrusions of the Tarim LIP have such low PGE concentrations.

Sulfide saturation and PGE enrichment in layered intrusions may be controlled by a number of factors, such as the degree of partial melting of the mantle, nature of parental magma, and magma chamber processes (e.g., Keays 1995; Li et al. 2001; Arndt et al. 2005). In this paper, we present a systematic study of PGE and Sr–Nd–Os isotopic compositions of the Mazaertag, Wajilitag, and Piqiang intrusions in the Tarim LIP. We compare the data with PGE-rich reefs of large layered intrusions in the world and examine the differences of the mantle sources and magma processes between PGE-poor and PGE-rich layered intrusions. Our study has general significance for better understanding the processes of sulfide saturation, PGE enrichment, and Fe–Ti oxide accumulation in layered intrusions. It is also helpful for evaluating the potentials of PGE mineralization in the Tarim LIP and geologically similar environments elsewhere.

Geological background

The Tarim LIP occurs in the Tarim basin in NW China and comprises diverse mafic-ultramafic volcanics and intrusions and felsic plutons, which are believed to have been formed from a mantle plume (e.g., Chen et al. 1997; Jia 1997; Jiang et al. 2004a, b, 2006; Borisenko et al. 2006; Tian et al. 2010; Zhang and Zou 2013a, b). The Tarim basin covers an area of ca. 530,000 km^2 and is surrounded by the Tianshan, Kunlun, and Altun orogenic belts (Fig. 1). The basement of the Tarim basin is composed of the late Neoarchean to early Paleoproterozoic high-grade metamorphic gneiss and amphibolite, and the late Paleoproterozoic to early Neoproterozoic volcanic-sedimentary

rocks and the late Neoproterozoic low-grade metamorphosed volcaniclastic rocks (Long et al. 2010; Zhang et al. 2012). The basement is overlain by a thick sedimentary sequence of Phanerozoic strata ranging in age from Ordovician to Neogene (XBGR 1993; Jia 1997). Mid-Neoproterozoic (830 to 620 Ma) felsic plutons and mafic-ultramafic intrusions mainly occur in the margin of the Tarim basin (Zhu et al. 2011; Ge et al. 2012; Zhang et al. 2013a).

The Tarim LIP is mainly composed of flood basalt, rhyolite, and mafic-ultramafic layered intrusions and syenitic and granitic plutons, as well as diamondiferous kimberlite, lamprophyre, mafic-ultramafic dikes, and bimodal dikes (Yang et al. 1996, 2006, 2007a, b, 2013; Chen et al. 1998; Jiang et al. 2004a, b; Zhang et al. 2008a, 2010a, b; Li et al. 2010; Wei and Xu 2011; Li et al. 2012a, b; Xu et al. 2014). The flood basalts are exposed in the northern, central, western, and southwestern parts of the Tarim Basin and cover an area of over 250,000 km^2 (Chen et al. 2006) (Fig. 1). The basaltic sequence varies from ca. 200 to 600 m with an average of ~300 m in thickness and is interlayered with thin sedimentary strata (Zhou et al. 2009; Yu et al. 2011). The flood basalts mainly consist of alkaline basalt, and minor picrite, trachybasalt, and andesitic/rhyolitic flows. The flood basalts are considered to have erupted in a short time span of 292–286 Ma and peaked at ~290 Ma (Wei et al. 2014a; Xu et al. 2014).

The mafic-ultramafic intrusions in the Tarim LIP were dated to be ~280 Ma (Zhang et al. 2010a; Qin et al. 2011; Su et al. 2011; Huang et al. 2012; Wei et al. 2014b). Some of the intrusions host Ni–Cu sulfide mineralization such as the Huangshanxi, Huangshandong, Tulargen, and Xiangshan
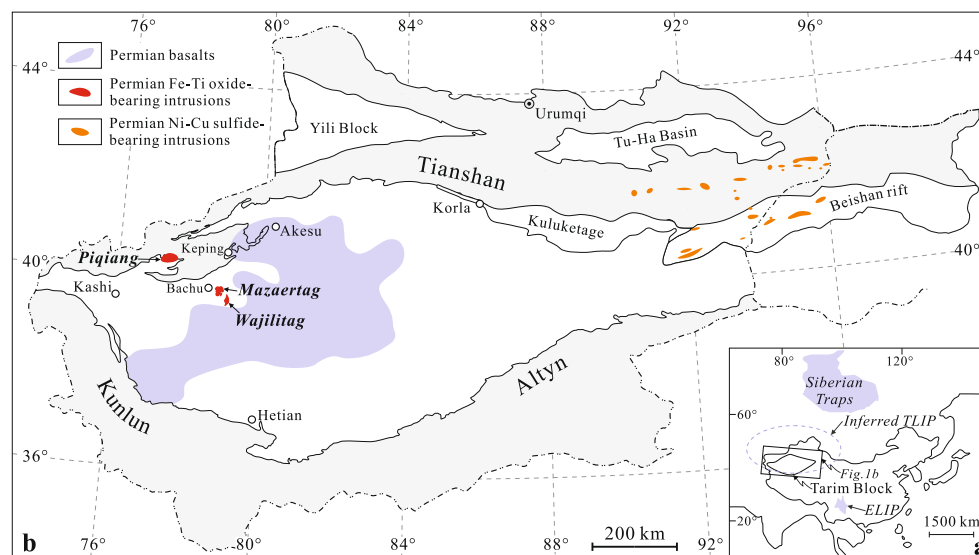

Fig. 1 Simplified geological map of the Tarim large igneous province showing the locations of the Mazaertag, Wajilitag, and Piqiang oxide-bearing intrusions and the distribution of the Tarim flood basalts and the sulfide-bearing mafic-ultramafic intrusions in the surrounding areas (after Xu et al. (2014) and Yang et al. (2014)). The *inset* shows the location of the Siberia Traps to the north and the Emeishan large igneous province (ELIP) to the south (after Zhou et al. (2009)), and the inferred extent of the Tarim large igneous province (TLIP) in Central Asia as suggested by Pirajno et al. (2009)

deposits in the northern Tianshan terrane (Qin et al. 2003; Zhou et al. 2004; Sun et al. 2008; Su et al. 2011; Gao and Zhou 2013; Sun et al. 2013), and the Baishiquan and Tianyu deposits in the Central Tianshan terrane (Chai et al. 2008; Tang et al. 2009), and the Hongshishan and Pobei complexes in the Beishan terrane (Mao et al. 2008; Pirajno et al. 2008; Su et al. 2009; Yang et al. 2014). Fe–Ti oxide-bearing layered intrusions such as the Mazaertag, Wajilitag, and Piqiang intrusions, occur in the western part of the Tarim Basin (Zhang et al. 2010c; Cao et al. 2014, 2015).

In the western part of the Tarim Basin, numerous NNW-trending mafic-ultramafic dikes intrude the Silurian, Devonian, Carboniferous, and lower Permian strata in the Bachu region (Zhou et al. 2009). Mafic-ultramafic dikes are extremely abundant in the Mazaertag and Wajilitag area and spatially associated with mafic-ultramafic intrusions and syenitic plutons (Zhang et al. 2008a; Yang et al. 2013; Zou et al. 2014). The dikes with nearly vertical dips also intrude the Xiaohaizi syenite, although some of the dikes intermingle with the syenite (Chen et al. 2010; Wei et al. 2014b). Bimodal dikes consisting of dolerite and quartz syenite porphyry are documented in several localities (Yang et al. 2007a). These dikes were dated to be between 272 and 284 Ma (Yu 2009; Li et al. 2011; Zou et al. 2014), coeval with the mafic-ultramafic intrusions and syenitic plutons in the region.

Fe–Ti oxide-bearing layered intrusions in the western part of the Tarim LIP

Mazaertag intrusion

The Mazaertag (also known as Xiaohaizi) intrusion has an outcrop area of ~0.13 km^2 (Fig. 2a). The intrusion mainly consists of olivine clinopyroxenite with interlayers of Fe–Ti oxide-bearing clinopyroxenite. The lithological classification for the rocks of the intrusion by Rui et al. (2002) is adopted in this study for the purpose of consistency. The contact between the olivine clinopyroxenite and the Fe–Ti oxide-bearing clinopyroxenite is transitional. The Mazaertag layered intrusion and adjacent syenitic pluton occur as a circular-shaped exposure of ~12.6 km^2 (Sun et al. 2009a). The Mazaertag intrusion is intruded by the syenite pluton, and the contact is sharp (Wei et al. 2014b). They both intrude the Silurian, Devonian, Carboniferous, and the lower Permian strata and form several 0.5- to 1-km-wide hornfels belts along the lower intrusive margin (XBGR 1993).

Olivine clinopyroxenite contains olivine (20–30 vol%), clinopyroxene (30–40 %), plagioclase (10–20 %), and Fe–Ti oxides (10–20 %). Euhedral to subhedral olivine and clinopyroxene crystals vary in size from 0.2 to 1 mm and 0.5 to 2.5 mm, respectively. Subhedral plagioclase laths range from 0.1 to 0.5 mm in width. Fe–Ti oxides occupy the angular

Fig. 2 **a** A simplified geological map of the Mazaertag intrusion (after ▶ Yang et al. (2007a) and Xu et al. (2014)). **b** A simplified geological map of the Wajilitag intrusion (after Rui et al. (2002)). **c** A cross section of the Wajilitag intrusion showing the major ore bodies in the intrusion (after Zhang et al. (2014)). **d** A simplified geological map of the Piqiang intrusion (after Zhang et al. (2014)). **e, f** Close-up and a cross section showing the distribution of lithological units and Fe–Ti oxide mineralization of the Piqiang intrusion (after Zhang et al. (2013b))

interstices between silicate mineral grains or are occasionally enclosed in olivine and clinopyroxene crystals (Fig. 3a).

Fe–Ti oxide-bearing clinopyroxenite consists of 10–20 % olivine, 30–40 % clinopyroxene, 10–20 % plagioclase, and 20–30 % Fe–Ti oxides. Fe–Ti oxide minerals occur either as small (3 mm) interstitial patches between the silicate minerals or as tiny inclusions in the silicate minerals. Some Fe–Ti oxide grains are rimmed by brown hornblende.
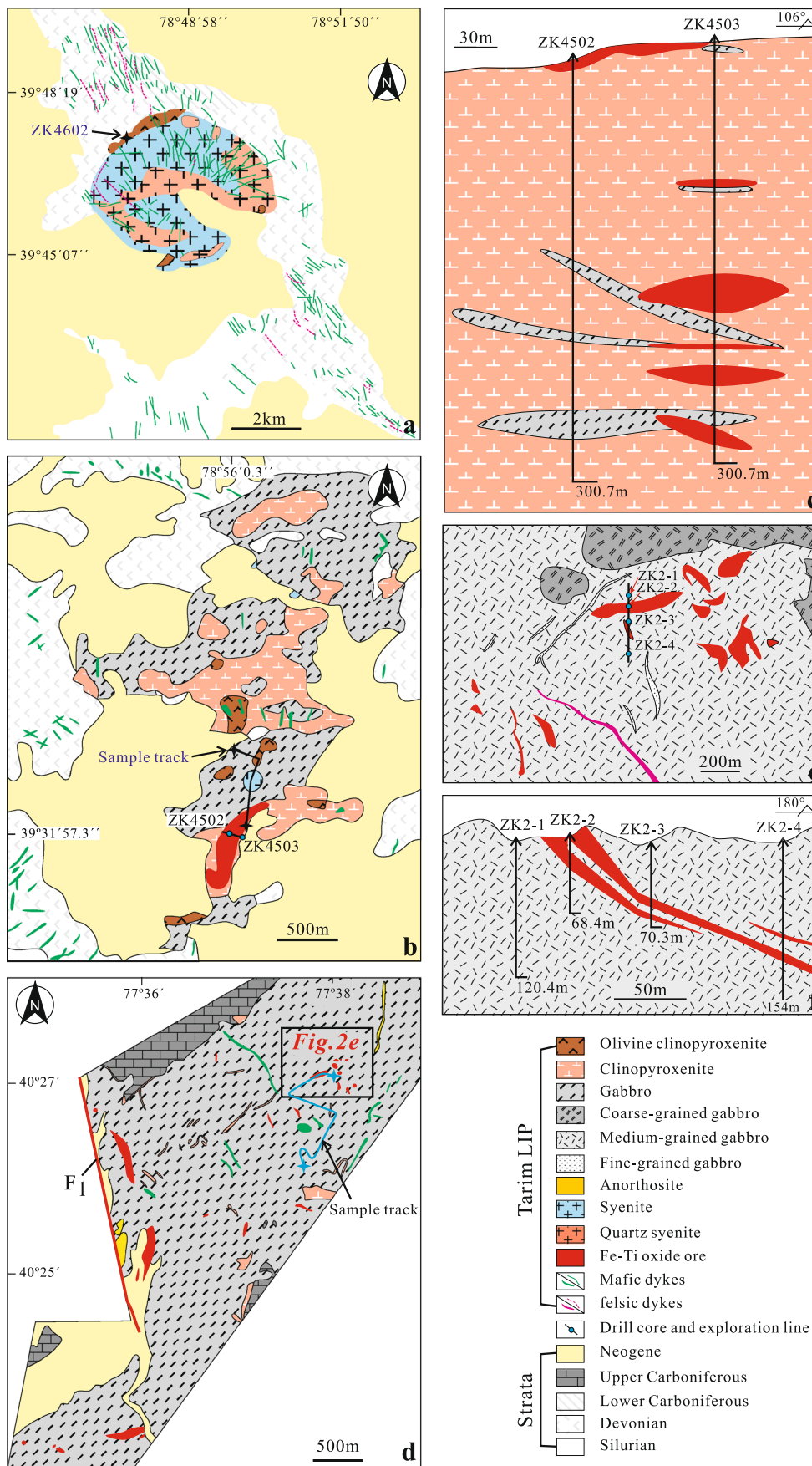
Both olivine clinopyroxenite and Fe–Ti oxide-bearing clinopyroxenite contain 1 to 3 % sulfides. The sulfides include pyrrhotite, pentlandite, and chalcopyrite (Fig. 3b–d). Polyphase sulfide blebs and patches are either interstitial to silicate minerals and Fe–Ti oxides (Fig. 3b–d) or are enclosed within margins of silicates (Fig. 3b) and Fe–Ti oxides (Fig. 3d).

Wajilitag intrusion

The 5-km-long, 1.5–3 km-wide, and 0.11–0.27-km-thick Wajilitag intrusion intrudes Silurian and Devonian sedimentary rocks (Fig. 2b). It consists of, from the base upward, olivine clinopyroxenite, coarse-grained clinopyroxenite, fine-grained clinopyroxenite, and gabbro. Lense-like or layered Fe–Ti oxide ore body extends for about 1.7 km long and 0.2–0.3 km wide and is mainly hosted in the fine-grained clinopyroxenite (Fig. 2b, c). The contact of the Fe–Ti oxide ore body and the host rock is transitional. The intrusion is overlain by syenitic plutons (Zhang et al. 2008a).

Olivine clinopyroxenite displays poikilitic texture and consists of olivine (10–15 %), clinopyroxene (50–60 %), plagioclase (10–20 %), Fe–Ti oxides (5–10 %), and minor apatite (<1 %). Olivine crystals are subhedral and vary from 0.3 to 2 mm in diameter. Clinopyroxene occurs as subhedral crystals and has size ranging from 0.5 to 3 mm. Plagioclase commonly occupies the angular interstices between olivine and clinopyroxene grains. Fe–Ti oxides are either enclosed in olivine and clinopyroxene or interstitial to silicate minerals.

Coarse-grained clinopyroxenite consists of clinopyroxene (75–80 %), Fe–Ti oxides (5–10 %), and olivine (<3 %). Subhedral to anhedral clinopyroxene grains have size ranging from 0.5×0.5 to 5×8 mm and contain two sets of ilmenite
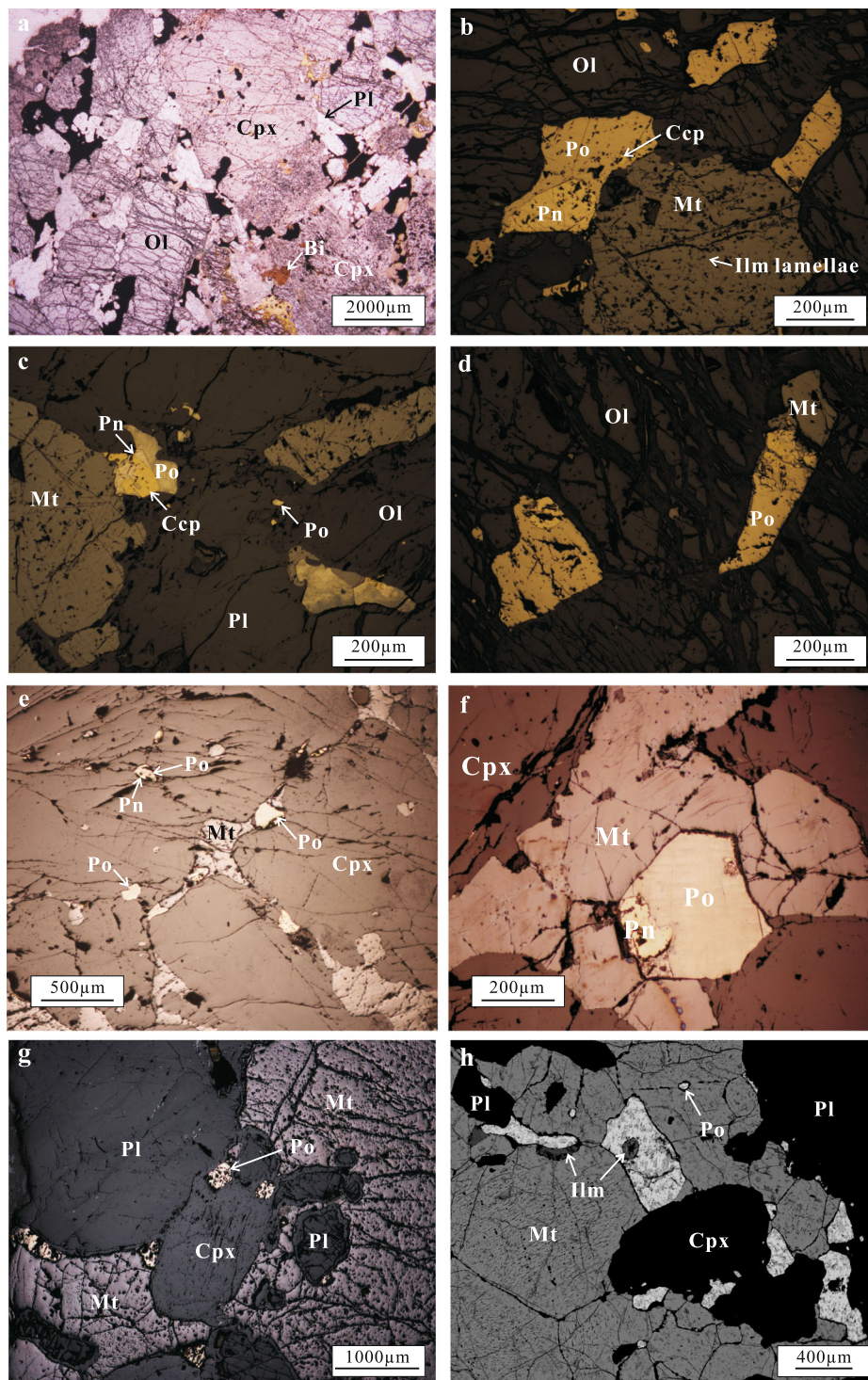
Fig. 3 a The olivine clinopyroxenite of the Mazaertag intrusion shows a poikilitic texture. Plane polarizer and transmitted light. Sample ZK4602-5. **b** The sulfides are interstitial to magnetite and cumulus olivines and are composed of pyrrhotite with pentlandite and chalcopyrite exsolutions. Reflected light. Sample ZK4602-5 from the Mazaertag intrusion. **c** Pyrrhotite bleb is enclosed in the margin of the plagioclase lath. Reflected light. Sample ZK4602-2 from the Mazaertag intrusion. **d** Intergrowth of magnetite and pentlandite in the olivine. Reflected light. Sample ZK4602-5 from the Mazaertag intrusion. **e** Pyrrhotite bleb is enclosed in the margin of the clinopyroxene. Reflected light. Sample BC1128 from the Wajilitag intrusion. **f** Pyrrhotite with pentlandite exsolutions are associated with magnetite in the interstitial phase. Reflected light. Sample BC1141 from the Wajilitag intrusion. **g** Pyrrhotite is interstitial to magnetite and silicate minerals. Reflected light. Sample PQ1102 from the Piqiang intrusion. **h** Pyrrhotite bleb is enclosed in the Fe–Ti oxides. BSE image. Sample PQ1105 from the Piqiang intrusion. *Ol* olivine, *Cpx* clinopyroxene, *Pl* plagioclase, *Mt* magnetite, *Po* pyrrhotite, *Pn* pentlandite, *Ccp* chalcopyrite

exsolution lamellae parallel to prismatic cleavage planes. Fe–Ti oxides occupy the interstice between clinopyroxene and olivine. Some olivine and clinopyroxene crystals contain small rounded inclusions of ilmenite and titanomagnetite.

Fine-grained clinopyroxenite contains clinopyroxene (70–85 %) and Fe–Ti oxides (15–20 %). Clinopyroxene crystals are about 0.5 × 0.5 mm in size. Fe–Ti oxides are interlocked with clinopyroxene.

Gabbro exhibits an ophitic texture and is composed of clinopyroxene (35–45 %), plagioclase (40–50 %), Fe–Ti oxides (<10 %), hornblende (<5 %), and apatite (<5 %). Small (0.1–0.75 mm) euhedral to subhedral apatite grains occur between the plagioclase laths, or they are enclosed in plagioclase laths.

The Fe–Ti oxide-rich clinopyroxenite contains 1 to 3 % sulfides, whereas other lithological units contain <1 % sulfides. Pyrrhotite is the major sulfide mineral, accounting for ~90 % of the sulfides. Pentlandite exsolved from pyrrhotite (Fig. 3e, f). Pyrrhotite blebs are enclosed within clinopyroxene grains in local places (Fig. 3e).

Piqiang intrusion

The Piqiang intrusion is a lens-like, EW-trending body and has an outcrop area of 16.7 km^2. It intrudes the late Carboniferous limestone and intercalated calcareous siltstone of the Kangkelin Formation (Fig. 2d). The intrusion is dismembered into two lobes by a NNW-trending fault (Fig. 2d). The east block is about six to eight times larger than that of west block (Zhou et al. 2010). Steeply dipping mafic and felsic dikes, a few tens of centimeters to ~5 m in width, intersect the intrusion and the country rocks of the Kangkelin Formation and lower Permian Bieliangjin Formation. The intrusion comprises six units from the base upward, including medium- to coarse-grained clinopyroxenite, coarse-grained gabbro, medium-grained gabbro, fine-grained gabbro, and medium- to coarse-grained anorthosite (cf. Rui et al. 2002; Zhang et al. 2013b). The medium-grained gabbro unit is underlain by a thin layer of olivine-rich gabbro. Small pods and dikes of anorthosite and fine-grained gabbro crop out sporadically (Fig. 2d, e). Internal contacts between the silicate rock units are gradational. Major Fe–Ti oxide ore bodies are hosted in the medium-grained gabbro unit (Fig. 2f) as concordant layers, lenses, and veins with thickness ranging from 1 to ~50 m.

Clinopyroxenite displays a granular texture and contains medium- to coarse-grained clinopyroxene (70–85 %), plagioclase (10–15 %), and Fe–Ti oxides (5–10 %). Small-grained clinopyroxene is subhedral

to euhedral and aggregated, whereas coarse-grained clinopyroxene crystals with zoning range in size from 2 to 4 mm. Some clinopyroxene crystals contain inclusions of euhedral or subhedral titanomagnetite. Plagioclase is tabular to platy with irregular wavy edges. Fe–Ti oxides appear to fill the interstices between silicates.

Coarse-grained gabbro consists of clinopyroxene (20–40 %), plagioclase (50–70 %), and Fe–Ti oxides (10–20 %). Plagioclase occurs as large crystals (2 to 7 mm) or small subrounded grains (0.4 to 1 mm). Subhedral clinopyroxene grains are 0.3 to 2 mm in size and contain ilmenite lamellae. Fe–Ti oxides occur as interstitial fillings between silicates.

Olivine gabbro shows a poikilitic texture and contains olivine (20 to 30 %), clinopyroxene (30 to 40 %), and plagioclase (30 to 40 %) with minor Fe–Ti oxides. Euhedral to subhedral olivine crystals vary in size from 0.1 to 3 mm in diameter. Clinopyroxene occurs as subhedral-anhedral crystals with diameter ranging from 0.2 to 2 mm. Plagioclase occupies angular interstices between olivine and clinopyroxene to form an intergranular texture. Fe–Ti oxides occur as blebs and patches in the interstitial spaces between silicates, or rounded inclusions in olivine and clinopyroxene crystals.

Medium-grained gabbro contains equigranular clinopyroxene and plagioclase crystals and 10–60 % interstitial Fe–Ti oxides, with minor olivine (<3 %). Olivine is typically subhedral to euhedral and varies in diameter from 0.3 to 1.5 mm. Clinopyroxene is euhedral and subhedral and ranges in size from 0.5 to 2.5 mm. Clinopyroxene displays extensive schiller exsolution of Fe–Ti oxides. Plagioclase laths range from 0.2 to 3 mm in length. The Fe–Ti oxide grains tend to occur in clusters about 5 mm in size. The clusters consist of a number of granular grains and locally form a matrix around silicate mineral grains.

Fine-grained gabbro contains clinopyroxene (35–50 %), plagioclase (40–50 %), and Fe–Ti oxides (10–25 %). Clinopyroxene occurs as euheral-subhedral crystals with diameter ranging from 1 to 4 mm. The clinopyroxene grains contain abundant ilmenite lamellae parallel to its prismatic cleavages. The aligned plagioclase crystals vary from 0.5 to 2.5 mm in size that define a predominant fabric in the rock. Fe–Ti oxides occur as 3 to 5 mm patches interstitial to the silicates.

Anorthosite is composed of ~90 % plagioclase with minor olivine, clinopyroxene, Fe–Ti oxides, hornblende, and biotite. Tabular plagioclase crystals vary in length from 1 to 6 mm. Olivine and clinopyroxene are interstitial to plagioclase. The reaction rim between Fe–Ti oxides and olivine primocrysts is

mainly composed of orthopyroxene. Fe–Ti oxides occupy the interstitial space between silicates, and a few Fe–Ti oxides are enclosed in olivine.

The Fe–Ti oxide-rich, medium-grained gabbro contains 1–3 % sulfides, whereas other rock types contain <1 % sulfide. In most cases, the dominant sulfide is pyrrhotite (Fig. 3g, h). The pyrrhotite occurs as isolated grains enclosed in the Fe–Ti oxides and silicates (Fig. 3g, h).

Sampling and analytical methods

The samples of the Wajilitag and Piqiang intrusions were collected from two open pits, and those of the Mazaertag intrusion were sampled from the drilled core ZK4602. The samples of the Tarim mafic-ultramafic dikes were collected from the outcrop in the Mazaertag area. The sample tracks of the Wajilitag and Piqiang intrusions and drilled core location of the Mazaertag intrusion are shown in Fig. 2a, b, d.

Fresh samples were selected and processed by jaw crusher and roller mill, and then powdered in agate mortars in order to minimize potential transition metal contamination.

Platinum-group elements were determined by isotope dilution-ICP-MS (Perkin-Elmer Sciex Elan6000) after PGE preconcentration using the method of Fe–Ni sulfide fire assay (Sun et al. 2009b) at Guangzhou Institute of Geochemistry, Chinese Academy of Sciences (GIGCAS). Each of spiked samples was mixed with 40 g $Na_2B_4O_7$, 2.5 g Fe, 1.0 g Ni, and 1.0 g S and fused in a clay crucible at 1000 °C for 60 min following the method of Ren et al. (2016). A sulfide bead was transferred to a glass beaker containing 15 ml H_2O for splitting into powder. With addition of 30 ml HCl, the sulfide powder was dissolved upon heating and insoluble residue was left. By filtration, the residue was collected and then transferred into a distillation apparatus with 3 ml HNO_3. Os was distilled at 110 °C for 30 min and simultaneously absorbed with 5 ml H_2O. The H_2O solution was analyzed by ICP-MS for Os. The remaining solution was concentrated and finally converted to 2 ml of 0.24 M HCl solution for loading to tandem columns packed with cation and Ln resins. Five milliliters of 0.24 M HCl eluent were collected for determination of Ru, Rh, Pd, Ir, and Pt by ICP-MS. For this method, the limits of detection (3σ for 20 g sample) for Os, Ir, Ru, Rh, Pt, and Pd are 0.7, 1, 2, 1.5, 6, and 25 ppt, respectively. The accuracy of this improved method was validated by analysis of a series of reference standards, and the results are generally in good agreement with their certified values (Table 2). Six duplicates for the samples with very low PGE concentrations from the Piqiang intrusion were analyzed in order to test the possible nugget

effect in these samples. The results are listed in Table 2 and indicate that the samples with very low PGE concentrations (<0.2 ppb Pd) may be more vulnerable to the nugget effect (cf. Savard et al. 2010). Therefore, only samples with Pd >0.2 ppb are plotted in the figures and used for discussion in this study. The precision of this method was then estimated to be better than 25 % for Os, 23 % for Ir, 22 % for Ru, 60 % for Rh, 3 % for Pt, and 5 % for Pd following the method of Ren et al. (2016).

Sulfur contents were determined by a PYRO cube Elemental Analyzer at the State Key Laboratory of Organic Geochemistry, GIGCAS. Analytical precision for S content was better than ±0.02 wt.%. The analytical results for PGE and S concentrations are presented in Table 2.

Whole-rock Os isotope compositions and Os concentrations were analyzed using a Triton negative thermal ionization mass spectrometer (NTIMS) in GIGCAS. The concentrations of Re in the rock samples were determined using a XSeries-2 quadrupole ICP-MS. Samples (1–3 g) were digested in Carius tubes using aqua regia following the method of Shirey and Walker (1995). After digestion, Os and Re were purified following the method of Birck et al. (1997). Os isotope fractionation was corrected using $^{188}Os/^{192}Os = 0.32440$. Both Re and Os were corrected for blanks. Total blank levels were 7.9 ± 2.6 and 0.7 ± 0.0 pg for Re and Os (2σ, $n = 8$), respectively, and the blank $^{187}Os/^{188}Os$ ratio was 0.2951 ± 0.0069 (2σ, $n = 8$). The contributions of the blanks to measured Os and Re contents were minor (<1 %). During our analysis, the WPR-1 standard yielded an average $^{187}Os/^{188}Os$ ratio of 0.14521 ± 28 (2σ, $n = 8$). The analytical results for Re and Os isotopic compositions are listed in Table 3.

Results

Whole-rock PGE and S concentrations

Samples from the Mazaertag and Wajilitag intrusions have total PGE concentrations ranging from 0.7 to 14.2 ppb, which is relatively higher than the Piqiang intrusion (total PGE = 0.4 to 2.3 ppb). The samples of the Tarim mafic-ultramafic dikes have total PGE of 0.7 to 4.3 ppb (Table 2). In the three intrusions, samples of Fe–Ti oxide-bearing and Fe–Ti oxide-poor rocks have similar PGE concentrations. All the rocks have a positive correlation of Pt and Pd (Fig. 4f) with Pd/Pt ratios ranging from 0.6 to 4.0.

Rocks of the Mazaertag and Wajilitag intrusions have S contents ranging from 1154 to 7073 ppm and from 151 to 1865 ppm, respectively, whereas the Piqiang intrusion have S contents varying from 157 to 6263 ppm. Samples of the Tarim mafic-ultramafic dikes have 190 to 930 ppm S. In the three intrusions, samples of the

Table 2 Compositions of platinum-group elements and selected trace elements for the rocks from the Wajilitag, Piqiang, and Mazaertag intrusions and Tarim mafic-ultramafic dikes

Sample	Ni (ppm)	Os (ppb)	Ir (ppb)	Ru (ppb)	Rh (ppb)	Pt (ppb)	Pd (ppb)	Cu (ppm)	S (wt%)	MgO (wt%)	Fe2O3T (wt%)	TiO2 (wt%)	Cr (ppm)	V (ppm)	Nb (ppm)	Th (ppm)	Yb (ppm)
Wajilitag intrusion																	
Olivine clinopyroxenite																	
BC1171	380	0.25	0.13	0.39	0.09	0.39	0.36	91.2	nd	14.1	17.1	3.68	624	385	25.5	2.19	1.47
BC1172	129	0.08	0.06	0.12	0.03	0.25	0.45	38.7	nd	7.44	15.2	4.04	187	332	56.8	4.37	2.20
BC1174	389	0.39	0.26	0.75	0.12	3.39	4.09	88.7	0.03	14.4	17.3	3.72	611	374	24.9	1.89	1.36
Coarse-grained clinopyroxenite																	
BC1115*	291	0.11	0.10	0.16	0.05	0.12	0.09	46.0	0.01	14.3	17.7	3.25	518	447	19.8	2.09	1.30
BC1117	239	0.16	0.15	0.24	0.06	0.36	0.51	36.7	0.02	12.1	16.5	3.69	414	401	31.4	3.33	1.46
Fine-grained clinopyroxenite																	
BC1147	146	0.15	0.19	0.20	0.09	1.00	1.25	368	0.19	11.0	23.6	7.79	321	754	10.3	0.10	1.20
Gabbro																	
BC1106	34.5	0.02	0.02	0.02	0.02	0.32	0.31	52.0	0.03	5.34	14.1	3.84	15.5	314	49.9	4.54	2.35
BC1108	17.8	0.02	0.01	0.03	0.01	0.22	0.59	47.6	0.05	4.82	14.5	3.89	4.38	314	61.2	5.29	2.31
BC1113*	4.78	0.01	0.002	0.01	0.01	0.10	0.15	60.1	0.02	2.84	8.67	2.39	5.78	819	6.65	1.79	3.13
Oxide clinopyroxenite																	
BC1125	235	0.26	0.62	0.94	0.02	4.90	7.42	247	0.06	10.7	26.7	8.32	288	824	6.55	0.07	1.02
BC1129	200	0.06	0.06	0.12	0.03	0.65	0.77	209	0.11	11.1	27.7	8.33	271	824	11.5	0.08	0.97
BC1131	206	0.13	0.16	0.30	0.04	1.17	2.02	183	0.05	11.5	25.8	7.59	239	789	10.2	0.27	0.97
BC1138	202	0.10	0.06	0.14	0.05	0.66	0.94	193	0.06	11.7	25.9	7.81	290	764	10.6	0.11	1.00
Piqiang intrusion																	
Clinopyroxenite																	
PQ1136*	141	0.003	0.004	0.01	0.02	0.08	0.14	31.4	0.03	10.3	17.2	1.97	179	277	2.63	0.50	1.50
Coarse-grained gabbro																	
PQ1203*	5.18	0.002	0.004	0.01	0.03	0.13	0.12	37.8	0.01	1.09	8.41	1.91	0.75	262	8.81	2.78	5.87
PQ03*	75.3	0.01	0.003	0.01	0.01	0.04	0.12	114	0.22	7.27	11.4	1.47	84.1	322	2.27	0.26	0.65
PQ1113	101	0.03	0.02	0.01	0.002	0.52	0.79	288	0.14	3.97	12.5	2.38	36.2	392	3.14	0.69	1.37
PQ1113R		0.01	0.03	0.01	0.02	0.48	0.74										
PQ1135*	52.2	0.002	0.01	0.01	0.02	0.15	0.14	47.7	0.01	5.00	13.0	2.45	37.0	510	6.02	0.88	0.86
PQ1146	29.0	0.03	0.01	0.02	0.003	0.31	0.45	184	0.23	4.91	15.9	3.68	7.00	590	2.86	0.15	0.55
PQ1147*	25.7	0.002	0.003	0.01	0.03	0.08	0.12	98	0.15	5.13	16.2	3.67	16.4	678	1.43	0.12	0.59
Olivine gabbro																	
PQ1174*	304	0.001	0.01	0.01	0.01	0.08	0.11	119	0.09	21.2	23.3	1.13	123	249	2.32	0.38	0.65
PQ1175*	289	0.003	0.004	0.01	0.04	0.08	0.12	76.7	0.07	20.8	23.2	1.19	159	256	2.69	1.57	0.82
PQ1206*	310	0.003	0.01	0.01	0.01	0.09	0.13	50.9	0.06	20.5	23.5	1.08	150	263	2.41	0.46	0.63
Medium-grained gabbro																	
PQ1131*	78.3	0.002	0.004	0.004	0.03	0.06	0.12	285	0.27	4.91	18.2	3.05	20.7	851	3.56	0.34	0.58
PQ1155	35.8	0.08	0.01	0.05	0.003	0.76	1.41	119	0.02	4.33	9.50	1.53	14.0	425	2.36	0.33	0.58
PQ1160*	30.9	0.001	0.003	0.003	0.03	0.14	0.08	80.6	0.10	2.87	7.88	1.34	13.7	309	3.00	0.36	0.43
PQ1165*	137	0.01	0.003	0.01	0.02	0.04	0.08	392	0.01	4.23	46.5	9.88	57.6	2673	6.55	0.15	0.34
PQ1173*	310	0.002	0.003	0.01	0.03	0.07	0.12	58	0.06	6.21	22.6	4.14	178	287	3.06	0.46	0.66
PQ1207*	146	0.01	0.01	0.01	0.03	0.19	0.13	89.4	0.01	12.3	22.2	2.68	183	694	1.84	0.14	0.66
PQ1207R		0.02	0.01	0.01	0.03	0.16	0.13										
PQ07*	16.5	0.01	0.002	0.01	0.02	0.05	0.10	54.4	0.06	4.70	8.32	1.47	13.2	233	1.58	0.26	0.70
Fine-grained gabbro																	
PQ1115*	46.9	0.01	0.01	0.01	0.003	0.04	0.15	238	0.12	4.72	18.3	3.49	20.4	862	2.25	0.13	0.52
PQ1152 * 36.0		0.001	0.003	0.004	0.02	0.05	0.09	203	0.01	6.19	20.2	4.07	22.2	1032	2.50	0.10	0.67
Anorthosite																	
PQ1141*	29.3	0.01	0.004	0.01	0.01	0.02	0.08	8.87	0.02	2.42	3.84	0.33	28.0	50.4	1.15	0.32	0.14
PQ1141R		0.01	0.01	0.02	0.02	0.02	0.09										
PQ1172*	32.1	nd	0.01	0.01	0.01	0.17	0.11	10.4	0.02	2.56	3.99	0.34	13.3	55.0	1.01	0.21	0.18
PQ1177*	20.3	0.01	0.01	0.01	0.01	0.04	0.14	5.91	0.02	1.85	2.90	0.26	18.9	31.5	1.99	0.53	0.15
Fe–Ti oxide ore																	
PQ1102*	125	0.01	0.03	0.05	0.02	0.06	0.11	362	0.55	4.84	61.3	14.0	65.9	3499	5.07	0.07	0.14
PQ1102R		0.01	0.02	0.09	0.02	0.13	0.11										
PQ1105*	141	0.01	0.004	0.01	0.01	0.05	0.11	330	0.46	4.17	69.8	16.0	46.2	2004	6.23	0.04	0.07
PQ1105R		0.01	0.004	0.02	0.03	0.04	0.19										
PQ1111*	111	0.004	0.004	0.01	0.02	0.07	0.12	302	0.44	5.93	51.2	11.0	34.8	2732	1.52	0.04	0.20
PQ1111R		0.01	0.01	0.01	0.02	0.15	0.16										
PQ1129	273	0.01	0.01	0.01	0.03	0.14	0.22	731	0.63	4.42	68.3	14.2	72.6	1909	6.69	0.02	0.06
PQ1127*	222	0.004	0.01	0.01	0.03	0.10	0.14	579	0.51	4.60	67.7	14.8	58.9	3281	0.15	0.06	0.13
Mazaertag intrusion																	
Olivine clinopyroxenite																	
ZK4602-1	560	0.14	0.23	0.20	0.10	1.74	3.03	92.6	0.50	17.9	21.7	2.80	787	376	4.47	0.27	0.57
ZK4602-2	566	0.13	0.20	0.44	0.07	1.82	1.34	44.2	0.12	19.8	20.5	2.17	749	324	2.79	0.20	0.51
ZK4602-5	633	0.17	0.16	0.21	0.07	0.75	1.10	39.5	0.12	22.0	21.3	1.99	937	299	3.47	0.25	0.49
ZK4602-6	419	0.17	0.14	0.32	0.06	0.49	1.09	88.9	0.16	18.2	20.4	2.40	783	375	3.13	0.17	0.53
ZK4602-8	432	0.36	0.10	0.10	0.05	0.79	1.01	114	0.20	17.6	21.5	2.84	618	459	3.74	0.47	0.61
ZK4602-9	594	0.11	0.37	0.41	0.15	1.58	2.73	356	0.59	17.1	23.1	3.12	577	510	2.29	0.08	0.51
Oxide clinopyroxenite																	
ZK4602-10	534	0.11	0.12	0.16	0.06	0.83	1.69	224	0.71	17.4	28.3	2.56	679	394	2.82	0.18	0.43

Table 2 (continued)

Sample	Ni (ppm)	Os (ppb)	Ir (ppb)	Ru (ppb)	Rh (ppb)	Pt (ppb)	Pd (ppb)	Cu (ppm)	S (wt%)	MgO (wt%)	Fe2-O3T (wt%)	TiO2 (wt%)	Cr (ppm)	V (ppm)	Nb (ppm)	Th (ppm)	Yb (ppm)
Tarim mafic-ultramafic dikes																	
Mafic dike																	
BC1121	43.9	0.02	0.02	0.03	0.02	0.33	0.26	55.2	0.09	5.31	15.2	4.03	77.7	376	58.1	7.25	2.30
BC1122	44.5	0.04	0.01	0.04	0.04	0.27	0.33	62.7	0.08	5.66	15.7	4.11	69.7	365	58.1	6.22	2.24
BC1134	12.5	0.01	0.29	0.51	0.10	1.42	1.95	75.6	nd	5.27	13.5	3.43	11.2	233	92.7	11.4	3.09
BC1155	154	0.04	0.01	0.05	0.05	0.26	0.42	81.7	0.06	6.91	13.7	2.84	215	292	30.9	3.58	1.85
BC1156	291	0.09	0.08	0.14	0.05	0.43	0.33	128	0.06	8.94	14.2	2.64	595	267	37.9	7.36	2.27
Ultramafic dike																	
BC1158	596	0.20	0.03	0.02	0.02	0.23	0.23	103	0.02	18.0	15.7	1.76	929	232	12.9	1.46	0.93
Standards																	
GPt-3	1	9.85	5.38	14.82	1.24	5.49	5.50										
	2	9.97	5.28	14.39	1.24	7.74	5.34										
	3	9.48	4.26	14.73	1.22	6.90	5.38										
	4	9.24	5.53	12.56	1.21	5.93	4.24										
	5	8.99	5.78	12.99	1.31	6.83	4.94										
	6	10.22	5.84	12.13	1.20	6.52	5.34										
	7	9.27	5.97	13.11	1.02	7.45	5.54										
	8	10.10	5.47	13.91	1.05	6.97	6.15										
	9	9.32	6.20	12.43	1.01	6.45	4.82										
	10	10.03	5.47	11.46	1.04	6.31	5.02										
	Average	9.65	5.52	13.30	1.15	6.76	5.22										
GPt-3	Certified	9.60	4.30	14.80	1.30	6.40	4.60										
GPt-2	1	0.06	0.03	0.08	0.06	1.59	2.09										
	2	0.06	0.03	0.06	0.06	1.49	2.40										
	3	0.05	0.03	0.08	0.06	1.50	1.96										
	4	0.07	0.03	0.06	0.05	1.30	2.38										
	5	0.06	0.02	0.06	0.07	1.71	2.40										
	Average	0.06	0.03	0.07	0.06	1.52	2.25										
GPt-2	Certified	0.06	0.05	(0.09)	0.10	1.60	2.30										
GBW07340	1	0.24	0.16	0.43	0.06	0.71	0.69										
	2	0.25	0.15	0.45	0.07	0.70	0.55										
	3	0.26	0.16	0.40	0.07	0.66	0.61										
	4	0.25	0.14	0.43	0.06	0.63	0.74										
	5	0.23	0.16	0.52	0.06	0.67	0.63										
	6	0.21	0.16	0.43	0.06	0.59	0.62										
	Average	0.24	0.15	0.44	0.06	0.67	0.64										
GBW07340	Reported	0.25	0.16	0.43	0.07	0.66	0.66										
Blank		0.005	0.005	0.01	0.01	0.08	0.14										

Certified values and reported values of the reference standards are from Sun et al. (2009b) and Savard et al. (2010), respectively. Samples with asterisk have Pd <0.02 ppb and large RSD between duplicates and are thus not included in the figures and discussion in the text in order to avoid the nugget effect in the samples. Data in parentheses are informational values. *nd means* not determined

nd not determined

Fe–Ti oxide ores have S content higher than the Fe–Ti oxide-poor rocks. There is a weak positive correlation of S and PGE for the rocks of the Mazaertag and Wajilitag intrusions, whereas there is a poor correlation of S and PGE for the rocks of the Piqiang intrusion (Fig. 5). Three samples from the coarse- and medium-grained gabbro in the Piqiang intrusion have high Pt and Pd concentrations relative to other samples at similar S content.

Samples from the three intrusions have a positive correlation of Cr with Ir and Pd (Fig. 6a, b), whereas they have a poor correlation of V with Ir and Pd (Fig. 6c, d). Samples from the Mazaertag intrusion have Cu/Pd ratios ranging from 3.1×10^4 to 1.3×10^5, whereas those of the Wajilitag intrusion have Cu/Pd ratios from 2.2×10^4 to 2.9×10^5. Samples of the Piqiang intrusion have Cu/Pd (8.4×10^4–3.3×10^6) much higher than

those of the Mazaertag and Wajilitag intrusions (Fig. 7a). Samples of the Tarim mafic-ultramafic dikes have Cu/Pd ratios (3.9×10^4–4.4×10^5) similar to those of the Wajilitag intrusion (Fig. 7a). Using the discrimination diagram for rocks formed under S-undersaturated and sulfide-saturated conditions (Vogel and Keays 1997), almost all the samples of the Wajilitag, Piqiang, and Mazaertag intrusions are plotted in the field, indicating that they formed from sulfide-saturated magmas (Fig. 7b).

Rocks of the Mazaertag and Wajilitag and the Tarim mafic-ultramafic dikes have trough-shaped patterns on the primitive mantle-normalized chalcophile element patterns, with a flat segment from Os to Ru and steep slope from Rh to Pd (Fig. 8a, b, d). Rocks of the Piqiang samples show steep-sloped patterns with positive Rh anomalies (Fig. 8c). Samples of the Piqiang intrusions have PGE patterns similar

Table 3 Re and Os isotopic compositions for the rocks from the Wajilitag, Piqiang and Mazaertag intrusions and the Tarim mafic-ultramafic dykes

	Re (ppb)	Os (ppb)	$^{187}Re/^{188}Os$	$^{187}Os/^{188}Os$	1σ	$(^{187}Os/^{188}Os)_i$	$\gamma_{Os}(t)$ (t=280 Ma)
Wajilitag intrusion							
Olivine clinopyroxenite							
BC1174	0.14	0.42	1.6340	0.1550	0.0002	0.1474	+18
BC1174-R	0.14	0.40	1.7140	0.1524	0.0004	0.1443	+15
Fine-grained clinopyroxenite							
BC1141	0.47	0.07	32.837	0.3252	0.0004	0.1717	+37
Gabbro							
BC1104	0.38	0.04	46.339	0.8682	0.0018	0.6515	+421
BC1106	0.12	0.06	9.1170	0.2424	0.0005	0.1998	+60
Oxide clinopyroxenite							
BC1123	0.70	0.15	23.461	0.2693	0.0003	0.1596	+28
Piqiang intrusion							
Clinopyroxenite							
PQ1136	0.22	0.00	458.56	2.9432	0.0134	0.7991	+539
Coarse-grained gabbro							
PQ1147	2.34	0.01	7789.5	37.425	0.1301	1.0034	+702
Medium-grained gabbro							
PQ1155	0.28	0.00	1323.3	13.750	0.0699	7.5628	+5944
Fine-grained gabbro							
PQ1152	0.23	0.01	430.30	12.360	0.0652	10.348	+8169
Fe-Ti oxide ore							
PQ1105	4.54	0.02	5692.0	24.752	0.1119	-	-
Mazaertag intrusion							
Olivine clinopyroxenite							
ZK4602-3	0.98	0.18	27.237	0.2694	0.0003	0.1420	+13
ZK4602-8	1.12	0.09	59.732	0.4326	0.0005	0.1533	+23
Oxide clinopyroxenite							
ZK4602-10	1.45	0.15	47.115	0.3705	0.0004	0.1502	+20
Tarim mafic-ultramafic dykes							
Mafic dyke							
BC1157	0.27	0.04	34.425	1.1544	0.0024	0.9935	+694
Ultramafic dyke							
BC1158	0.22	0.45	2.3800	0.1749	0.0002	0.1638	+31

to most samples of the Tarim flood basalts but have much depleted Os, Ir, and Ru (Fig. 8c). The rocks of the Mazaertag and Wajilitag intrusions have PGE patterns similar to those of the Fe–Ti oxide-bearing, layered intrusions in the Emeishan LIP (Fig. 8a, b).

Whole-rock Sr–Nd and Re–Os isotopes

The Tarim mafic-ultramafic dikes have relatively constant $\varepsilon_{Nd}(t = 280$ Ma$)$ values ranging from −0.5 to +2.9 and initial $^{87}Sr/^{86}Sr$ ratios from 0.7047 to 0.7054 (Table 4; Fig. 9). Samples from three intrusions have initial $^{87}Sr/^{86}Sr$ and $\varepsilon_{Nd}(t)$ values similar to the Tarim mafic-ultramafic dikes, but overall have $\varepsilon_{Nd}(t)$ values higher

and initial $^{87}Sr/^{86}Sr$ lower than those of the Tarim flood basalts (Fig. 9).

Samples of the Tarim mafic-ultramafic dikes have 0.22–0.27 ppb Re and 0.04–0.45 ppb Os, and they have $^{187}Re/^{188}Os$ of 2.38–34.42 and $^{187}Os/^{188}Os$ of 0.17–1.15. Samples of the Mazaertag intrusion have initial $^{187}Os/^{188}Os$ ratios of 0.27 to 0.43 and $\gamma_{Os}(t = 280$ Ma$)$ values of +13 to +23. Samples of the Wajilitag intrusion have 0.04 to 0.40 ppb Os and 0.12–0.70 ppb Re with $^{187}Re/^{188}Os$ of 1.6–46.3 and $^{187}Os/^{188}Os$ of 0.15–0.87. They have $\gamma_{Os}(t)$ values varying from +15 to +421 (Table 3). On the other hand, samples of the Piqiang intrusion contain 0.22 to 4.54 ppb Re and 0.003 to 0.016 ppb Os, and they have $^{187}Re/^{188}Os$ varying from 430 to 7789 and $^{187}Os/^{188}Os$ from 2.94 to 37.4 with large

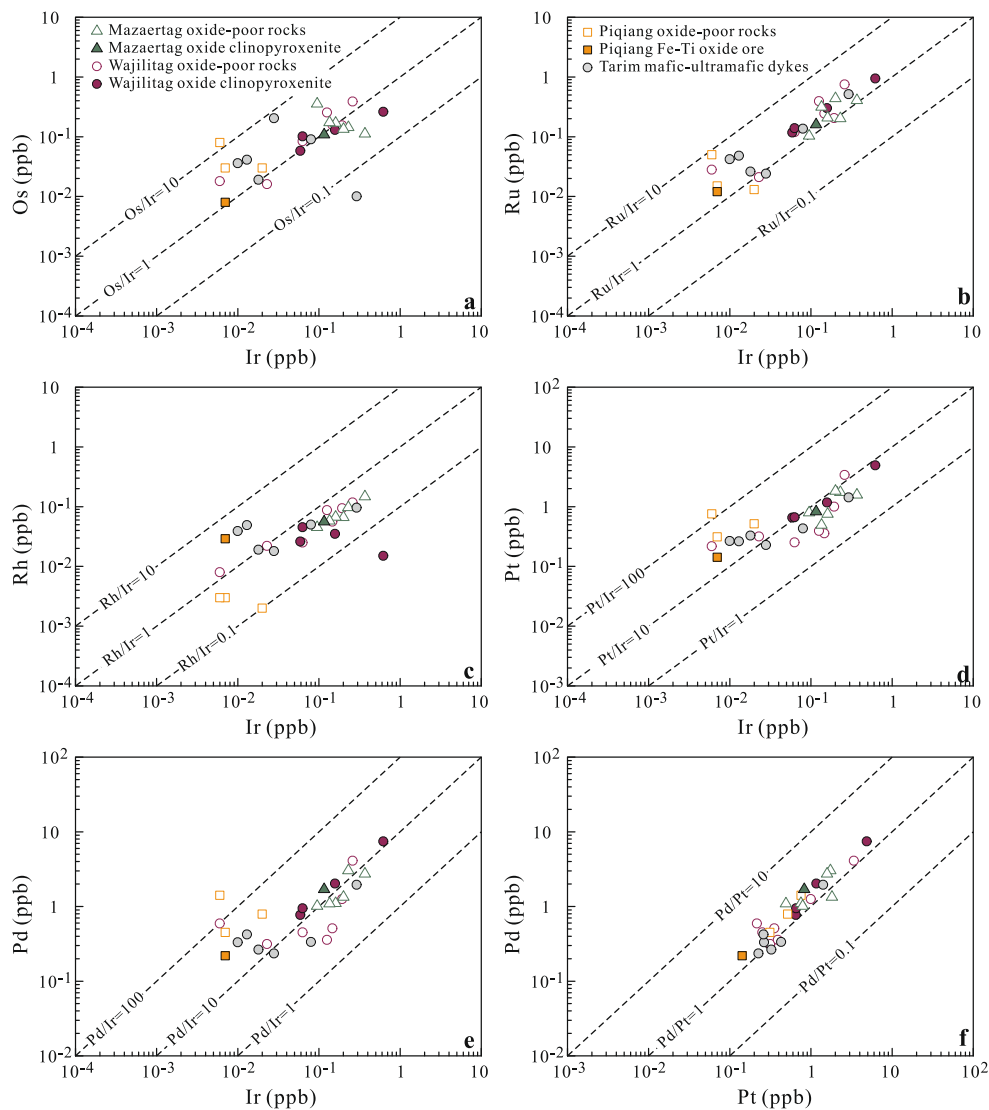**Fig. 4** Plots of Ir versus Os (**a**), Ru (**b**), Rh (**c**), Pt (**d**), and Pd (**e**), and Pt versus Pd (**f**)

uncertainty, which probably resulted from the underestimation of analytical uncertainty or post-magmatic disturbance of the Re–Os isotope system (Lambert et al. 2000). Therefore, these data cannot be used for the calculation of initial Os isotopic compositions.

Discussion

No contribution of lithospheric mantle to the formation of Fe–Ti oxide-bearing layered intrusions

Interaction of mantle-derived magma with the subcontinental lithospheric mantle (SCLM) may play a significant role in the genesis of magmatic ore deposits (cf. Griffin et al. 2013). Previous small degrees of partial melting would not dissolve all sulfides in the mantle

so that a second-stage melting of a metasomatized SCLM would produce PGE-rich magma because of scavenging PGE from the retained sulfides in the SCLM (Maier and Grove 2011). It is observed that magmatic Ni–Cu-(PGE) deposits are often associated with the "fertile" LIPs showing geochemical evidence consistent with contamination by ancient metasomatized SCLM (Zhang et al. 2008b). The Noril'sk-Talnakh Ni–Cu-(PGE) sulfide deposits are considered to be related to the generation of the Siberian Traps due to the interaction of a mantle plume with the lithosphere mantle (Begg et al. 2010).

The parental magmas of the major PGE-mineralized layered intrusions worldwide have significant SCLM component (Begg et al. 2010; Maier and Grove 2011). The chilled zone of the Skaergaard intrusion has $\gamma_{Os}(t)$ of −5 (Fig. 10), which is interpreted as the interaction to
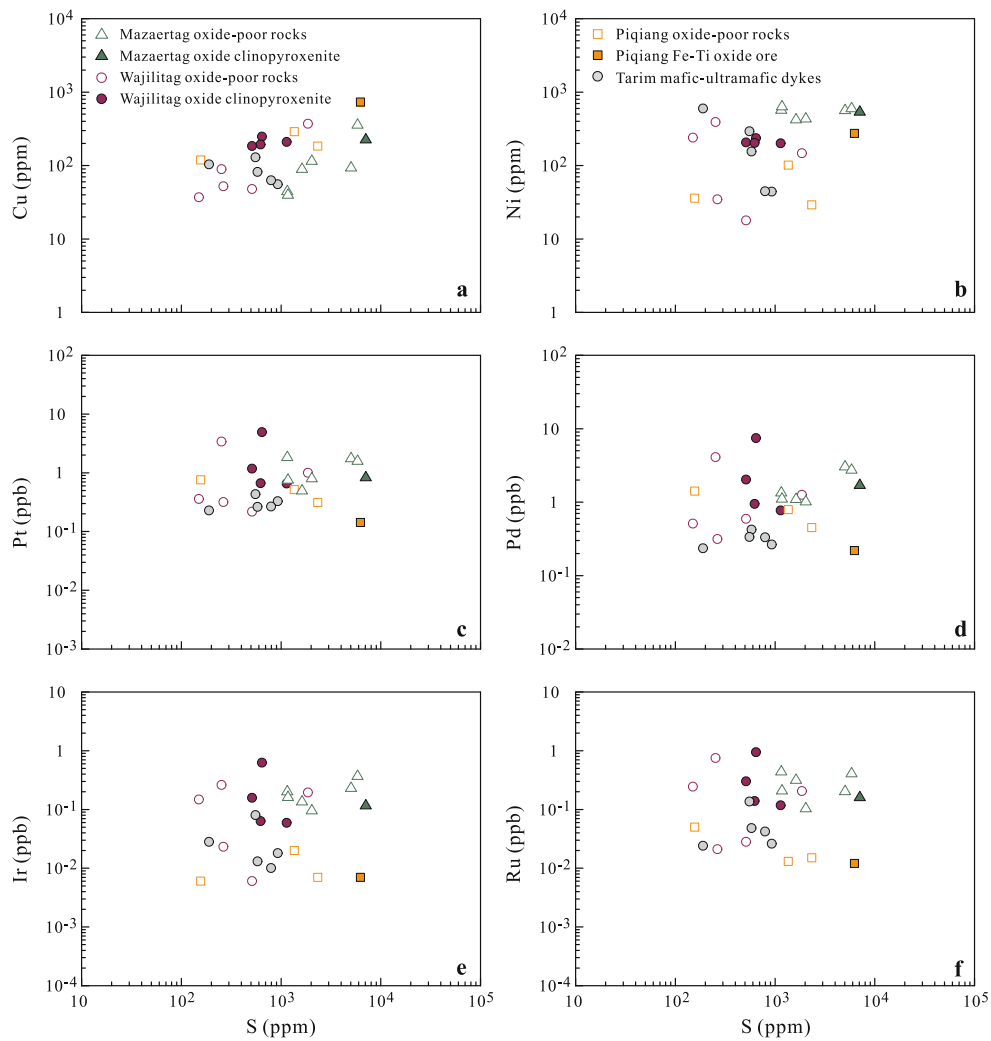
Fig. 5 Covariations of Cu, Ni, and PGE with S. Samples from the Wajilitag and Mazaertag intrusions and the Tarim mafic-ultramafic dikes exhibit positive correlations of Pt and Pd with S, whereas the samples from the Piqiang intrusion show no correlation of PGE and S

an extent with ancient SCLM (Brooks et al. 1999). The chromite from the marginal zone of the Bushveld Complex has near-chondritic Os isotopic compositions with $\gamma_{Os}(t)$ ranging from −0.8 to +3.1, consistent with a derivation from an ascending plume-derived magma contaminated by ancient SCLM (Curl 2001). The chromitite seams in the Ultramafic series of the Stillwater Complex have $\gamma_{Os}(t)$ of −2 to +4.1, which is also interpreted as the involvement of SCLM in the petrogenesis (Lambert et al. 1994). The rocks of the Stella intrusion exhibit nearly flat REE and Th/Ta of 0.5 to 3.3 (Maier et al. 2003), comparable with those of Andean arc basalts that have weak fractionated LREE/HREE and Th/Ta of 3.8 (Kelemen et al. 2004). The Stella intrusion intruded the Kraaipan greenstone belt (Maier et al. 2003), which consists of metamorphosed mafic volcanic rocks interlayered with ferruginous and phyllitic metasedimentary rocks (Poujol et al. 2002). Given that the Kraaipan greenstone belt

may represent the Archean suture of protocratonic nuclei (Poujol et al. 2002; Said et al. 2010), the geochemical features of the Stella intrusion were considered to indicate a depleted SCLM component (Begg et al. 2009) in its mantle source.

A SCLM component was also proposed for Fe–Ti oxide-bearing layered intrusions in the Emeishan LIP. The parental magmas of the Fe–Ti oxide-bearing layered intrusions in the Emeishan LIP are considered to be of Fe–Ti-rich basaltic which was derived from high-Ti picritic magma from an enriched mantle source (Wang et al. 2014). The Xinjie Fe–Ti oxide-bearing layered intrusion has $\gamma_{Os}(t)$ of −0.7 to −0.2 (Zhong et al. 2011). The picritic dikes in the Panzhihua Fe–Ti oxide-bearing layered intrusion have $\gamma_{Os}(t)$ of −0.1 to +2.8 (Hou et al. 2013). Both are considered to be consistent with the addition of SCLM into the Emeishan plume-derived high-Ti magmas. The Fe–Ti oxide-bearing layered intrusions in
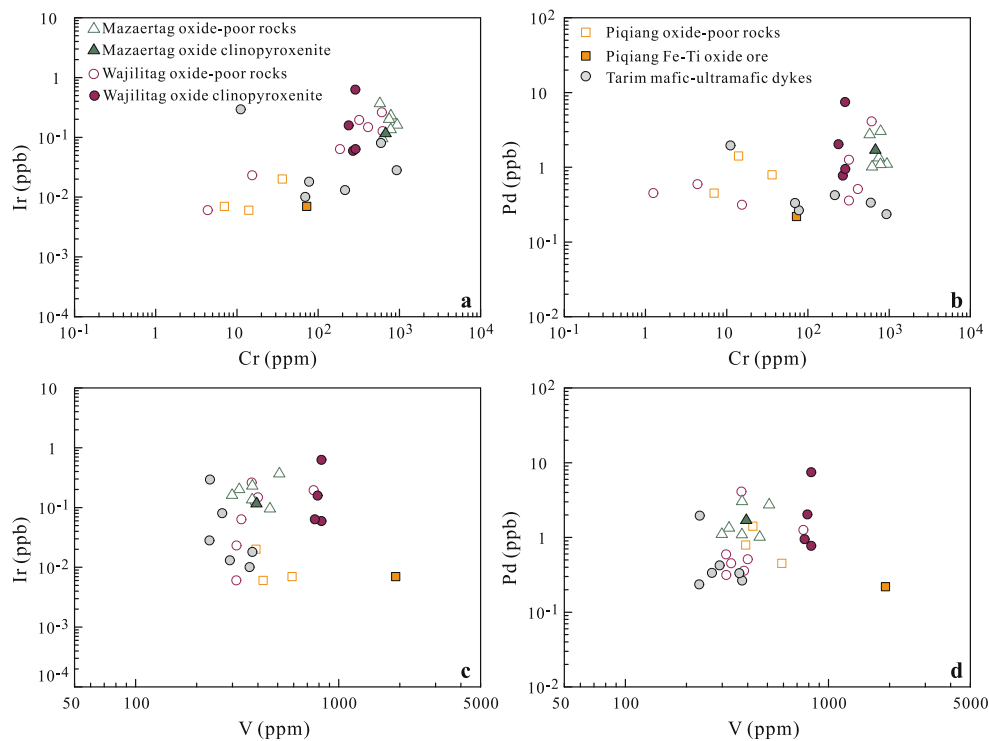
Fig. 6 Binary plots of Cr with Ir (**a**) and Pd (**b**) and V with Ir (**c**) and Pd (**d**)

the Emeishan LIP contain 36 wt% FeO and 12.6 wt% TiO_2 on the average (Zhou et al. 2008) and minor PGE-rich layers, which is considered to be a result of the assimilation of Fe- and Ti-rich SCLM into the Emeishan mantle plume (cf. Hou et al. 2013).

The layered intrusions in the Tarim LIP were believed to have been derived from an OIB-like mantle source (Zhang et al. 2010a). The rocks of the Mazaertag and Wajilitag intrusions have enriched LILE, HFSE, and LREE on the primitive mantle-normalized trace element patterns (Cao et al. 2014; Wei et al. 2014b). They have low $(^{87}Sr/^{86}Sr)_i$ (0.7037 to 0.7051) and high ε_{Nd} (−0.4 to +3.9) relative to the bulk silicate Earth (Fig. 9). The least contaminated samples from the Mazaertag and Wajilitag intrusions have slightly radiogenic initial Os isotope signatures and $\gamma_{Os}(t)$ values of +13 to +23, and they have $(Nb/Th)_{PM}$ of 1.5 to 1.9 and $(Th/Yb)_{PM}$ of 2.4 to 8.1 (Cao et al. 2014 and our unpublished data for the Mazaertag intrusion). These geochemical features are well compared with those for OIB (cf. Sun and McDonough 1989; Walker et al. 1997). The slightly radiogenic $\gamma_{Os}(t)$ and $\varepsilon_{Nd}(t)$ values for the rocks of the Mazaertag and Wajilitag intrusions therefore indicate that the parental magmas of the intrusions may have been derived from a convecting mantle source, as previously suggested by Wei et al. (2014a) and Xu et al. (2014).

The mafic-ultramafic dikes in the Bachu region have $(^{87}Sr/^{86}Sr)_i$ ratios ranging from 0.7038 to 0.7079 and

$\varepsilon_{Nd}(t)$ values from −1.1 to +5.2, similar to that of the OIB-like mantle-derived rocks (Zhou et al. 2009; Wei et al. 2014a). The Sr–Nd isotopic compositions of the mafic-ultramafic dikes are overlapped the field for the layered intrusions in the Tarim LIP in the plot of $(^{87}Sr/^{86}Sr)_i$ versus $\varepsilon_{Nd}(t)$ (Fig. 9), indicating that they may have been derived from the same mantle source. In addition, the uncontaminated mafic dikes in the Bachu region have $(Nb/Th)_{PM}$ of 1.2–1.5 and $\varepsilon_{Nd}(t)$ of +4.3 to +4.8 (Wei et al. 2014b), nearly identical to the proposed plume component for the Emeishan high-Ti basalts with $(Nb/Th)_{PM}$ of 1.0–1.1 and $\varepsilon_{Nd}(t)$ of +4.6 to +4.8 (Xu et al. 2001). The most primitive ultramafic dike in this region have $(Nb/Th)_{PM}$ of 1.0 and $\gamma_{Os}(t)$ of +31. Therefore, the mafic-ultramafic dikes in this region may have been derived from a convecting mantle source.

The Tarim LIP experienced a prolonged igneous activity from ca. 300 to 272 Ma (Xu et al. 2014). Two main magmatic episodes are identified; the first episode is marked by ~290 Ma Tarim flood basalts, whereas the second episode is ~280 Ma ultramafic-mafic-felsic intrusions and mafic-ultramafic dikes (Wei et al. 2014a; Xu et al. 2014). The rocks generated in the two episodes have distinct geochemical compositions. The ~290 Ma Tarim flood basalts have $\varepsilon_{Nd}(t)$ values ranging from −9.2 to −1.8, which have been proposed to be derived from a long-term enriched SCLM source (Zhou et al. 2009; Zhang et al. 2010a; Li et al. 2012b; Wei et al.
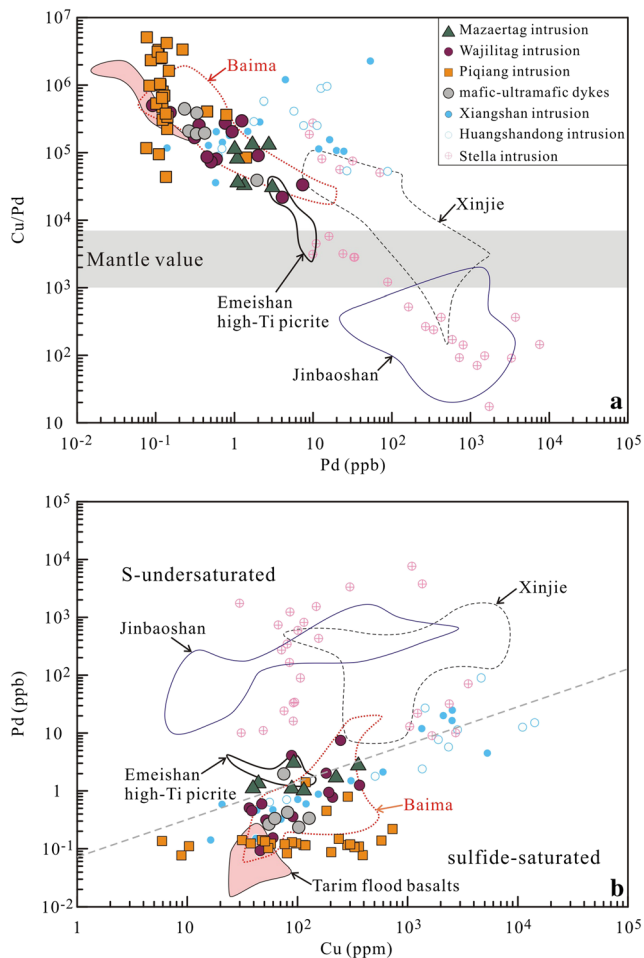
Fig. 7 **a** Plot of Cu/Pd versus Pd, and **b** plot of Cu versus Pd for the samples from the Mazaertag, Wajilitag, and Piqiang intrusions showing that almost all the samples formed from sulfide-saturated magmas (cf. Vogel and Keays 1997). Data sources: mantle value after Barnes et al. (1993); Tarim flood basalts in the Sishichang and Yingan sections after Yuan et al. (2012) and Li et al. (2012b); Emeishan picrites after Bai et al. (2012) and Li et al. (2012c); Baima Fe–Ti oxide-bearing layered intrusion (Baima) after Zhang et al. (2013c); Xinjie layered intrusion with Fe–Ti oxide and Pt–Pd mineralization (Xinjie) after Zhong et al. (2011); Jinbaoshan Pt–Pd deposit (Jinbaoshan) after Wang et al. (2010); Stella Pt–Pd deposit after Maier et al. (2003); Xiangshan layered intrusion with Fe–Ti oxide and Ni–Cu sulfide mineralization after Sun et al. (2008) and Xiao et al. (2013); and Huangshandong mafic–ultramafic intrusion with Ni–Cu sulfide mineralization after Sun et al. (2013)

2014a). On the other hand, the ~280 Ma mafic-ultramafic intrusions such as Mazaertag, Wajilitag, and Piqiang have $\varepsilon_{Nd}(t)$ values much higher than those for the Tarim flood basalts (Fig. 9), indicating that these mafic-ultramafic intrusions may have been derived from the mantle source different from that for the Tarim flood basalts. The Tarim mantle plume that had incubated at the base of the Tarim craton is considered to have provided the heat for triggering the melting of the enriched SCLM components at ~290 Ma, whereas the decompressional

melting of the mantle plume without SCLM component produced ~280 Ma intrusive bodies (Xu et al. 2014). This is consistent with the fact that some LIP magmas may have passed through the SCLM without appreciable modification (Day et al. 2008), which is probably the main reason that the layered intrusions in the Tarim LIP contain insignificant PGE mineralization.

Sulfide retention in the mantle

The rocks in the Mazaertag, Wajilitag, and Piqiang intrusions have very low PGE concentrations (Table 2) relative to the primitive mantle and therefore have Cu/Pd much higher than that of the primitive mantle (Fig. 7a). The ultramafic dike in this region is considered to represent the compositions of relatively primary magma of the Tarim LIP (Zhou et al. 2009). The most primitive ultramafic dike contains 0.7 ppb PGE, which is significantly lower than that of the Emeishan high-Ti picrites (15.2–27 ppb; Bai et al. 2012; Li et al. 2012c), indicating that the primitive magma of these intrusions are likely PGE-depleted.

Both Pd and Cu are highly incompatible elements and will therefore build up in the residual melts (Keays 1995). Because Pd is highly compatible in sulfide, Cu/Pd ratio of the rocks will be higher than the mantle value of ~7000 if there is a retention of the sulfide in the mantle source or an early removal of sulfide melt during magma ascent (Barnes and Picard 1993; Bennett et al. 2000). The samples of the Mazaertag, Wajilitag, and Piqiang intrusions have Cu/Pd ratios much higher than the mantle values (Fig. 7a). However, the samples from the Mazaertag and Wajilitag intrusions have relatively constant Cu/Pd (Fig. 7a), similar to the minimum Cu/Pd ratio of the Piqiang intrusion. The samples from each intrusion have more restricted Cu/Pd than those for the Stella intrusion but have the range of Cu/Pd similar to those for the Xiangshan and Huangshandong Ni–Cu sulfide-bearing intrusions in East Tianshan (Fig. 7a). The high Cu/Pd and overall PGE depletion for the rocks of the Mazaertag, Wajilitag, and Piqiang intrusions are thus attributed to early-stage sulfide segregation, either in the mantle or during the evolution of magmas en routine to the magma chamber where they emplaced.

It has been suggested that the mantle contains ~250 ppm S (McDonough and Sun 1995) or 0.054 wt% sulfide (Lorand 1993). The minimum degree of partial melting to complete dissolution of the sulfide in the mantle are considered to be 11–25 % depending on the S contents of different mantle sources (Keays 1995; Naldrett 2010; Lightfoot et al. 2012). The least evolved mafic dike (W13) in the Bachu region have Mg# of ~56
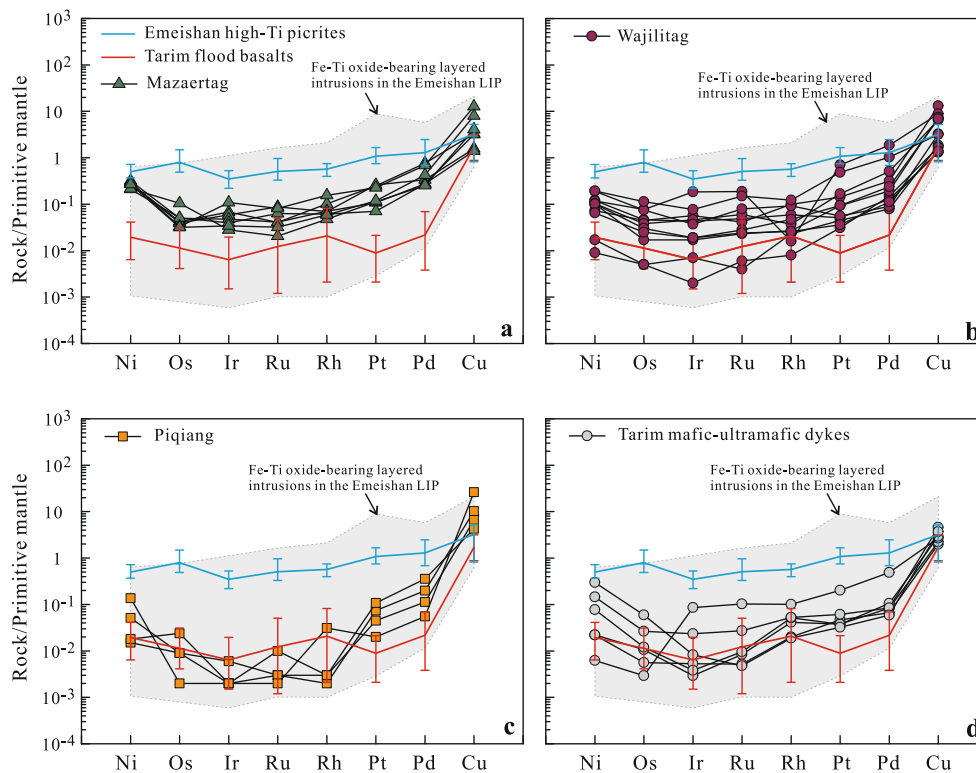
Fig. 8 Primitive mantle-normalized chalcophile element patterns for the samples from the Mazaertag, Wajilitag and Piqiang intrusions and the Tarim mafic-ultramafic dikes. Normalization values of the primitive mantle are from Barnes and Maier (1999). Data sources: the Tarim flood basalts (Li et al. 2012b; Yuan et al. 2012); the Emeishan picrites (Bai et al. 2012; Li et al. 2012c); the Emeishan Fe–Ti oxide-bearing layered intrusions, the Panzhihua intrusion (Howarth and Prevec. 2013); Honge intrusion (Bai et al. 2012) and Baima intrusion (Zhang et al. 2013c)

and is assumed to be the analogue to the parental magma of the Wajilitag intrusion (Zhang et al. 2008a; Cao et al. 2014). The parental magma of the Piqiang intrusion is considered to have the composition similar to the mafic dikes in the Piqiang region (Zhang et al. 2010a). The mafic dikes in both Bachu and Piqiang region have Nb/Y ranging from 0.92 to 1.97 and have affinity of alkaline basalts (Zhou et al. 2009; Zhang et al. 2010a; Wei et al. 2014a).

Early-crystallzed olivine or clinopyroxene in these intrusions can be used to estimate the compositional features of the parental melts (Driouch et al. 2010). Clinopyroxene contains most of the incompatible trace elements and is suitable for the estimation of the compositions of the parental magmas (Bédard 2014). However, the major and trace element concentrations of clinopyroxene could be modified by the re-equilibration of the crystal and trapped intercumulus liquids if the proportion of the trapped liquid is significant in the cumulates (Charlier et al. 2005; Godel et al. 2011; Cawthorn 2013). As REE are incompatible in both silicate minerals and coexisting Fe–Ti oxides in the Mazaertag, Wajilitag, and Piqiang intrusions, we chose La

concentrations of the rocks to estimate the proportions of trapped liquids for each sample. Most samples from the Mazaertag, Wajilitag, and Piqiang intrusions contain 5 ppm La (Cao et al. 2014, 2015 and our unpublished data for Mazaertag). The averaged concentration of La for the Tarim mafic dikes (44.9 ppm; Zhang et al. 2010a) is adopted to represent the liquid composition, the proportions of the trapped liquid in the samples are estimated to be ranging from ~0 to 11 % in maximum, typically with 7 %. Such minor amount of the trapped liquid may have negligible effect on the incompatible element compositions of the clinopyroxene. The composition of the clinopyroxene in the Mazaertag, Wajilitag, and Piqiang intrusions can thus be used for the reversed calculation to obtain the compositions of the melts that were in equilibrium with the clinopyroxene. The results indicate that the calculated melts for the three intrusion have trace element patterns similar to the high-Ti flood basalts of the Emeishan LIP, and the averaged compositions of the mafic dikes in the Bachu and Piqiang regions (Fig. 11a), which are consistent with the low degrees (<10 %) of partial melting of the mantle source (Fig. 11b). This may explain the low PGE concentrations of the rocks in the three intrusions as sulfide

Table 4 Sr and Nd isotopic compositions for the rocks from the Wajilitag, Piqiang and Mazaertag intrusions and Tarim mafic-ultramafic dykes

	Rb (ppm)	Sr (ppm)	$^{87}Rb/^{86}Sr$	$^{87}Sr/^{86}Sr$	±2σ	$(^{87}Sr/^{86}Sr)_i$	Sm (ppm)	Nd (ppm)	$^{147}Sm/^{144}Nd$	$^{143}Nd/^{144}Nd$	±2σ	$\varepsilon_{Nd}(t)$
Wajilitag intrusion												
Olivine clinopyroxenite												
BC1171[a]	12.3	696	0.051	0.703970	0.000014	0.7038	9.09	44.6	0.123	0.512630	0.000006	+2.5
BC1172[a]	29.4	1181	0.072	0.704960	0.000013	0.7047	14.1	72.9	0.117	0.512550	0.000007	+1.1
BC1174	9.27	669	0.040	0.703970	0.000012	0.7038	8.63	41.2	0.127	0.512630	0.000008	+2.4
Fine-grained clinopyroxenite												
BC1141[a]	2.18	164	0.039	0.704350	0.000012	0.7042	10.1	36.2	0.168	0.512729	0.000007	+2.8
Gabbro												
BC1104[a]	33.9	744	0.132	0.704950	0.000012	0.7044	10.6	51.4	0.125	0.512558	0.000007	+1.0
BC1106	30.8	1101	0.081	0.704677	0.000014	0.7044	14.0	71.8	0.118	0.512475	0.000009	-0.4
Oxide clinopyroxenite												
BC1123[a]	0.24	75.7	0.009	0.704410	0.000014	0.7044	4.89	16.4	0.180	0.512712	0.000006	+2.0
BC1131[a]	1.25	99.2	0.036	0.704610	0.000013	0.7045	5.08	18.5	0.166	0.512707	0.000007	+2.5
Piqiang intrusion												
Clinopyroxenite												
PQ1136[b]	2.78	181	0.044	0.706440	0.000013	0.7063	3.75	14.3	0.158	0.512481	0.000013	-1.7
Coarse-grained gabbro												
PQ1146[b]	1.69	444	0.011	0.705250	0.000017	0.7052	1.24	4.40	0.171	0.512640	0.000010	+1.0
PQ1147[b]	1.32	453	0.008	0.705340	0.000012	0.7053	1.39	4.50	0.186	0.512606	0.000013	-0.2
Olivine gabbro												
PQ1174[b]	2.61	148	0.051	0.706410	0.000012	0.7062	1.32	5.03	0.159	0.512500	0.000014	-1.3
PQ1175[b]	3.69	149	0.071	0.706320	0.000014	0.7060	1.76	6.59	0.162	0.512470	0.000009	-2.0

The data for samples with a, b are cited from Cao et al. (2014) and Cao et al. (2015), respectively. The initial isotopic ratios were calculated at 280 Ma

may have been retained in the mantle in the low degrees of partial melting of the mantle.

Crustal contamination and sulfide saturation

The continental crust has a radiogenic Os isotopic composition with $^{187}Os/^{188}Os >0.8$ due to high Re/Os ratios of the continental crust (Esser and Turekian 1993). Therefore, the mantle-derived magma may have elevated $^{187}Os/^{188}Os$ ratios if it is interacted with crustal material, especially those with low Os content (Widom and Shirey 1996; Shirey and Walker 1998). Such interaction will not significantly disturb the lithophile element isotopic systematics such as Rb–Sr and Sm–Nd systems (Schoenberg et al. 2003).

The extent of crustal contamination of the magmas from which the three intrusions formed can thus be estimated using initial $^{87}Sr/^{86}Sr$ ratios and $\varepsilon_{Nd}(t)$ values of the bulk rocks, assuming that the rock compositions observed are products of the mixing of a mantle-derived magma and a crustal contaminant. We used the least evolved composition of the Bachu mafic dike as the mantle-derived end member. For the crustal end-member, we used the averaged composition of the Proterozoic gneiss and gneiss granite in the Tarim Block (after Hu et al. 2006), representing the lower crust and upper crust of the Tarim Block, respectively (Fig. 9). The modeling results indicate that the parental magmas of the Mazaertag

and Wajilitag intrusions experienced <10 % contamination of the upper crust (Fig. 9). This is consistent with that the Mazaertag and Wajilitag intrusions have averaged initial $^{187}Os/^{188}Os$ of 0.1485 and 0.1646 just slightly higher than the estimated value of 0.1251 for the primitive upper mantle (Meisel et al. 2001).

The rocks of the Piqiang intrusion may have experienced ~15 to 25 % contamination of the upper crust (Fig. 9). The rocks from the Piqiang intrusion have Cu/Pd ranging from 8.4×10^4 to 3.3×10^6, much higher than those for Mazaertag ($3.1 \times 10^4 - 1.3 \times 10^5$) and Wajilitag ($2.2 \times 10^4 - 2.9 \times 10^5$), indicating that the rocks of the Piqiang intrusion had experienced intensive sulfide segregation during magma ascent and significant amounts of PGE may have been left behind at depth. Therefore, the rocks of the Piqiang intrusion have PGE concentrations much lower than those of the rocks in the Mazaertag and Wajilitag intrusions (Fig. 8 and Table 2).

Magnetite crystallization and sulfide saturation

Tiny sulfides that are in coexistence with the magnetites are commonly observed in the Mazaertag, Wajilitag, and Piqiang intrusions (Fig. 3), similar to the association of sulfide and magnetite in the Stella intrusion (Maier et al. 2003), the Skaergaard intrusion (Holwell and Keays 2014), and the Rincón del Tigre Complex (Prendergast
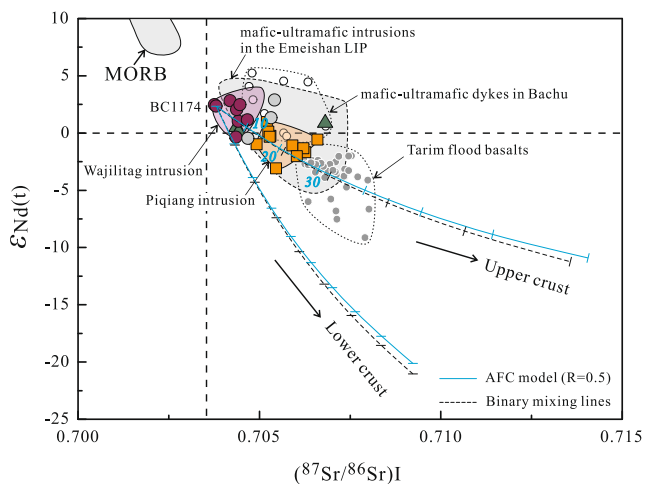
Fig. 9 Plot of $(^{87}Sr/^{86}Sr)_i$ and $\varepsilon Nd(t)$ values for the rocks from the Mazaertag, Wajilitag, and Piqiang intrusions and Tarim mafic-ultramafic dikes. The initial $^{87}Sr/^{88}Sr$ and $\varepsilon Nd(t)$ values for the three intrusions and Tarim mafic-ultramafic dikes are recalculated to 280 Ma, and those for the Tarim flood basalts are recalculated to 290 Ma. Data sources: the Tarim mafic-ultramafic dikes from Zhou et al. (2009) and Wei et al. (2014a); the Tarim flood basalts from Zhou et al. (2009), Li et al. (2012b), and Wei et al. (2014a). The field of the Wajilitag intrusion after Cao et al. (2014) and the Piqiang intrusion after Cao et al. (2015). Emeishan Fe–Ti oxide-bearing intrusions from a compilation by Pang et al. (2010). Mid-oceanic ridge basalts (MORBs) from Zindler and Hart (1986). Sample BC1174 from the Wajilitag intrusion is used as the starting composition for the parental magma. The upper crust and lower crust represented by the Tarim Proterozoic gneiss granite and Proterozoic paragneiss given in Hu et al. (2006). The *numbers* indicate the percentages of participation of the crustal materials. The calculated parameters of Nd (ppm), $\varepsilon Nd(t)$, Sr (ppm), and $(^{87}Sr/^{86}Sr)_i$ are 29, – 24, 76, 0.771 and 51, – 26, 444, 0.711 as two components of the Tarim upper and lower crust. The value of R is the rate of assimilation/rate of crystallization. $D^{Sr} = 0.7207$ and $D^{Nd} = 0.6382$, which is calculated for an assemblage with olivine, clinopyroxene, plagioclase, and Fe–Ti oxides = 6/40/38/16 using D values in Rollinson (1993). The ticks for binary mixing and AFC model line are shown at 0.1 intervals. Symbols are the same as those in Fig. 6. The trends observed in the data are explained by an AFC process; the same is not true for bulk mixing, which is shown for comparison

2000). As a result of decompression during upwelling that increased the solubility of sulfide in the magma (Mavrogenes and O'Neill 1999), the originally sulfide-saturated magma would become sulfide undersaturated when it ascends into the crust. In this case, sulfide saturation would occur after substantial crystallization in a closed system or after the addition of crustal S during contamination (Mavrogenes and O'Neill 1999; Li and Ripley 2005). As crustal contamination did not play an important role in the sulfide saturation of the Mazaertag and Wajilitag intrusions, sulfide saturation in the shallow magma chamber may be mainly controlled by fractional crystallization.

The PGE mineralization in the Stella and Skaergaard intrusions and the Rincón del Tigre Complex is considered to be
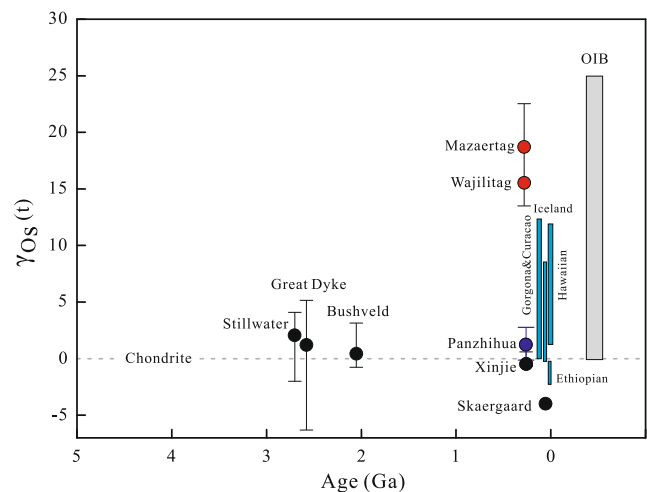

Fig. 10 Plot of $\gamma_{Os}(t)$ versus age for the major PGE-mineralized and PGE-unmineralized layered intrusions worldwide and the Mazaertag and Wajilitag intrusions. The *horizontal dashed line* represents the evolution of the chondritic average. The value for the modern ocean island basalts (OIBs; compiled by Walker et al. 1997) is shown for reference. Data sources: Bushveld complex after Curl (2001); Stillwater complex after Lambert et al. (1994); Great Dyke after Schoenberg et al. (2003); Skaergaard intrusion after Brooks et al. (1999); Xinjie intrusion after Zhong et al. (2011); Panzhihua intrusion after Hou et al. (2013)

related to a prolonged fractionation of the magma (~60 % at Stella and Skaergaard intrusion; Andersen et al. 1998; Maier et al. 2003) such that the PGE deposits occur in the upper portions of the magma chambers (Holwell and Keays 2014). As shown in Fig. 10, the parental magmas of the layered intrusions in the Tarim LIP have trace element patterns similar to the Emeishan high-Ti basalts, which are considered to be analogue to the parental magma of the Fe–Ti oxide-bearing, layered intrusions in the Emeishan LIP (e.g., Zhou et al. 2008; Pang et al. 2010). Due to the absence of primitive magma compositions of the Tarim LIP, the representative composition of the high-Ti picrite of the Emeishan LIP (Kamenetsky et al. 2012) was chosen to illustrate the effects of fractional crystallization on S contents and sulfide saturation of residual basaltic liquids. MELTS modeling indicates that ~54 % of crystallization is required to induce sulfide saturation without addition of crustal S (Fig. 12), and that sulfide saturation may achieve when magnetite joins plagioclase and clinopyroxene as a liquidus phase. This is supported by the occurrence of small sulfide inclusions enclosed within interstitial magnetite (Fig. 3d). The degree of magma fractionation in the Tarim LIP is quite similar to the calculation for the Baima intrusion in the Emeishan LIP, which is ~59 % fractionation of a picritic magma (Zhang et al. 2013c). Hence, we consider that the prolonged fractional crystallization with magnetite crystallization may have played an important role in the sulfide saturation of the Mazaertag and Wajilitag magma systems.
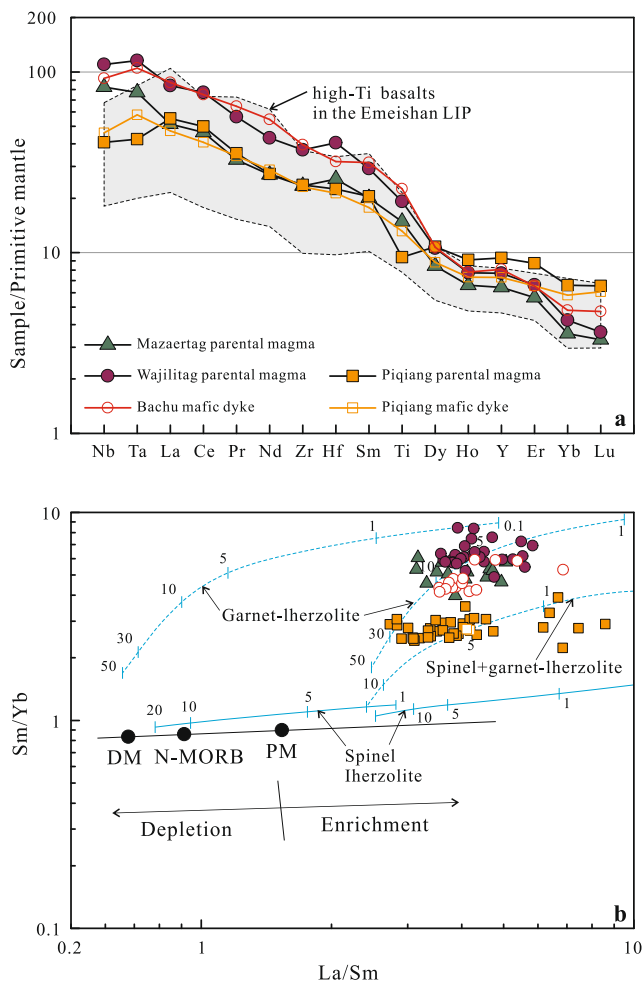
Fig. 11 **a** Primitive mantle-normalized trace element patterns for the melt compositions calculated from the clinopyroxenes for the Mazaertag, Wajilitag, and Piqiang intrusions, which are compared with those for the whole-rock compositions of the selected mafic dikes. The compositions of the clinopyroxene are listed in Electronic Supplementary Material Table 1. The Cpx/melt partition coefficients adapted the value by Hart and Dunn (1993), Hauri et al. (1994), Lundstrom et al. (1998), Hill et al. (2000, 2011), and Gaetani et al. (2003) (Electronic Supplementary Material Table 2). Data sources: Emeishan high-Ti basalts (Xu et al. 2001; Qi et al. 2008); Bachu mafic dike (Zhou et al. 2009, their sample XHZ36); Piqiang mafic dike (Zhang et al. 2010a, their sample 08KT01-15). **b**-La/Sm versus Sm/Yb diagram showing the melting curves for the parental magmas of the Mazaertag, Wajilitag, and Piqiang intrusions (after McKenzie and O'Nions (1991)), indicating that their parent magmas were derived from <10 % partial melting. The lines are nonmodal fractional melting curves for garnet lherzolite and spinel lherzolite. *Numbers on the lines* refer to percentages of melt. DM depleted mantle, PM primitive mantle, N-MORB normal mid-ocean ridge basalt

Fig. 12 Modeling of the sulfur content at sulfide saturation (SCSS) with fractional crystallization assuming a primitive high-Ti picritic magma. Fractional crystallization is simulated using the MELTS program (Ghiorso and Sack 1995) at a total pressure of 1 kbar and $fO_2 = FMQ$, the starting composition was adapted the melt inclusion in the olivine of the high-Ti picrites in the Emeishan LIP with the composition of 46.38 wt.% SiO_2, 2.25 wt.% TiO_2, 7.91 wt.% Al_2O_3, 12.29 wt.% FeO, 0.07 wt.% MnO, 19.68 wt.% MgO, 9.25 wt.% CaO, 1.41 wt.% Na_2O, 0.40 wt.% K_2O, 0.18 wt.% P_2O_5, 0.07 wt.% S; sample M8 62, Kamenetsky et al. 2012. The SCSS in the silicate melt is calculated using the equation of Li and Ripley (2009)

Conclusions

The Mazaertag, Wajilitag, and Piqiang Fe–Ti oxide-bearing, mafic-ultramafic layered intrusions were sourced from a convecting, OIB-like mantle source, without appreciable input of SCLM component. The parental magmas of the three intrusions were PGE-depleted due to low degrees of partial melting of the mantle source. Although sulfide saturation occurred in the late stage of crystallization and was associated with the crystallization of magnetite, the potentials for PGE mineralization in the Tarim LIP are low. It is likely that prospective PGE-rich layered intrusions may form due to a suite of combined factors including (1) interaction of the mantle-derived magmas with SCLM component, (2) high degrees of partial melting of the mantle, (3) insignificant crustal contamination of the magma, and (4) sulfide saturation of the parental magma due to a prolonged fractional crystallization.

As discussed above, the parental magmas of the three layered intrusions in the Tarim LIP may have been sulfide-saturated before the differentiation of the magma in shallower magma chamber, and PGE may have been retained in the mantle due to the low degrees of partial melting of the mantle. In this case, although the late-stage sulfide saturation of the magma will cause sulfide segregation, chance to form economic important PGE deposits is uncertain.
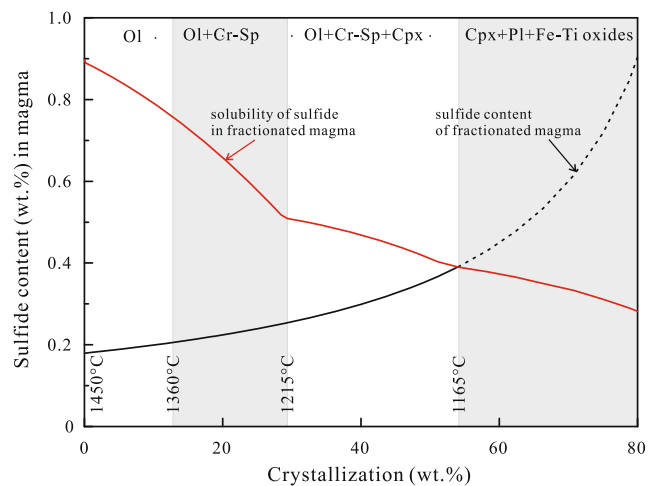
References

Andersen JCØ, Rasmussen H, Nielsen TFD, Ronsbo JG (1998) The Triple Group and the Platinova gold and palladium reefs in the Skaergaard intrusion: Stratigraphic and petrographic relations. Econ Geol 93:488–509

Arndt NT, Lesher CM, Czamanske GK (2005) Mantle-derived magmas and magmatic Ni-Cu-(PGE) deposits. In: Hedenquist JW, Thompson JFH, Goldfarb RJ, Richards JP (eds) Economic Geology One Hundredth Anniversary Volume, pp 5–24

Bai ZJ, Zhong H, Li CS, Zhu WG, Xu GW (2012) Platinum-group elements in the oxide layers of the Hongge mafic–ultramafic intrusion, Emeishan large igneous province, SW China. Ore Geol Rev 46: 149–161

Barnes SJ, Maier WD (1999) The fractionation of Ni, Cu and the noble metals in silicate and sulfide liquids. In: Keays RR, Lesher CM, Lightfoot PC, Farrow CEG (eds) Dynamic processes in magmatic ore deposits and their application to mineral exploration. Geol Assoc Can (Short Course Notes) 13:69–106

Barnes SJ, Picard CP (1993) The behavior of platinum-group elements during partial melting, crystal fractionation, and sulfide segregation: an example from the Cape Smith Fold Belt, northern Quebec. Geochim Cosmochim Acta 57:79–87

Barnes SJ, Maier WD, Ashwal AD (2004) Platinum-group elements distribution in the Main and Upper zone of the Bushveld Complex. Chem Geol 208:293–317

Bédard JH (2014) Parameterizations of calcic clinopyroxene-Melt trace element partition coefficients. Geochem Geophy Geosys 15:303–336

Begg GC, Griffin WL, Natapov LM, O'Reilly SY, Grand S, O'Neill CJ, Poudjom Djomani Y, Deen T, Bowden P (2009) The lithospheric architecture of Africa: Seismic tomography, mantle petrology and tectonic evolution. Geosphere 5:23–50

Begg GC, Hronsky JAM, Arndt NT, Griffin WL, O'Reilly SY, Hayward N (2010) Lithospheric, cratonic and geodynamic setting of Ni-Cu-PGE sulphide deposits. Econ Geol 105:1057–1070

Bennett VC, Norman MD, Garcia MO (2000) Rhenium and platinum group element abundances correlated with mantle source components in Hawaiian picrites: sulphides in the plume. Earth Planet Sci Lett 183:513–526

Birck JL, Roy-Barman M, Capmas F (1997) Re–Os isotopic measurements at the femtomole level in natural samples. Geostandard Newslett 21:19–27

Borisenko A, Sotnikov V, Izokh A, Polyakov G, Obolensky A (2006) Permo-Triassic mineralization in Asia and its relation to plume magmatism. Russ Geol Geophys 47:170–186

Brooks CK, Keays RR, Lambert DD, Frick LD, Nielsen TFD (1999) Re–Os isotope geochemistry of Tertiary picritic and basaltic magmatism of East Greenland: constraints on plume- lithosphere interactions and the genesis of the Platinova reef, Skaergaard intrusion. Lithos 47:107–126

Buchanan DL, Nolan J, Suddaby P, Rouse JE, Viljoen MJ, Davenport JWJ (1981) The genesis of sulfide mineralization in a part of the Potgietersrus limb of the Bushveld Complex. Econ Geol 76:568–579

Campbell IH, Naldrett AJ (1979) The influence of silicate:sulphide ratios on the geochemistry of magmatic sulfides. Econ Geol 74:1503–1505

Campbell IH, Naldrett AJ, Barnes SJ (1983) A model for the origin of the platinum-rich sulfide horizons in the Bushveld and Stillwater Complexes. J Petrol 24:133–165

Cao J, Wang CY, Xing CM, Xu YG (2014) Origin of the early Permian Wajilitag igneous complex and associated Fe-Ti oxide mineralization in the Tarim large igneous province, NW China. J Asian Earth Sci 84:51–68

Cao J, Wang CY, Xing CM, Xu YG (2015) Whole-rock and mineral compositions of the Piqiang Fe-Ti oxide-bearing mafic-ultramafic intrusion in the early Permian Tarim large igneous province, NW China: magma fractionation processes and accumulation of Fe-Ti oxides. (in preparation)

Cawthorn RG (2013) Rare earth element abundances in apatite in the Bushveld Complex − a consequence of the trapped liquid shift effect. Geology 41:603–606

Charlier B, Vander Auwera J, Duchesne JC (2005) Geochemistry of cumulates from the Bjerkreim- Sokndal layered intrusion (S. Norway). Part II: REE and the trapped liquid fraction. Lithos 83: 255–276

Chen HL, Yang SF, Dong CW (1997) The discovery of early Permian basic rock belt in the Tarim basin and its tectonic meaning. Geochimica 26:77–87 (in Chinese with English abstract)

Chen HL, Yang SF, Jia CZ, Dong CW, Wei GQ (1998) Confirmation of Permian intermediate-acid igneous rock zone and a new understanding of tectonic evolution in the northern part of the Tarim Basin. Acta Mineral Sin 18:370–376 (in Chinese with English abstract)

Chen HL, Yang SF, Wang QH, Luo JC, Jia CZ, Wei GQ, Li ZL, He GY, Hu AP (2006) Sedimentary response to the early-mid Permian basaltic magmatism in the Tarim plate. Chin Geol 33:545–552 (in Chinese with English abstract)

Chen MM, Tian W, Zhang ZL, Guan P (2010) Geochronology of the Permian basic-intermediate -acidic magma suite from Tarim, northwest China and its geological implications. Acta Petrol Sin 26:559–572 (in Chinese with English abstract)

Curl EA (2001) Parental magmas of the Bushveld Complex, South Africa. Ph.D thesis, Monash University, Australia, pp 107–108

Day JMD, Pearson DG, Hulbert LJ (2008) Rhenium–Osmium isotope and platinum-group element constraints on the origin and evolution of the 1.27 Ga Muskox layered intrusion. J Petrol 49:1255–1295

Driouch Y, Béziat D, Grégoire M, Laguenini F, Abbou MB, Ntarmouchant A, Roddaz M, Dahire M, Bennouna A, Belkasmi M, Brusset S, Debat P (2010) Clinopyroxene trace element compositions of cumulate mafic rocks and basalts from the Hercynian Moroccan Central Meseta: petrogenetic implications. J Afr Earth Sci 56:97–106

Esser BK, Turekian KK (1993) The osmium isotopic composition of the continental crust. Geochim Cosmochim Acta 57:3093–3104

Gaetani G, Kent AR, Grove T, Hutcheon I, Stolper E (2003) Mineral/melt partitioning of trace elements during hydrous peridotite partial melting. Contrib Mineral Petrol 145:391–405

Gao JF, Zhou MF (2013) Generation and evolution of siliceous high magnesium basaltic magmas in the formation of the Permian Huangshandong intrusion (Xinjiang, NW China). Lithos 162–163: 128–139

Ge RF, Zhu WB, Zheng BH, Wu HL, He JW, Zhu XQ (2012) Early Pan-African magmatism in the Tarim Craton: insights from zircon U–Pb–Lu–Hf isotope and geochemistry of granitoids in the Korla area, NW China. Precambrian Res 212–213:117–138

Ghiorso MS, Sack RO (1995) Chemical mass transfer in magmatic processes IV. A revised and internally consistent thermodynam ic model for the interpolation and extrapolation of liquid–solid equilibria in magmatic systems at elevated temperatures and pressures. Contrib Mineral Petrol 119:197–212

Godel B, Barnes SJ, Maier WD (2011) Parental magma composition inferred from trace element in cumulus and intercumulus silicate minerals: an example from the Lower and Lower Critical zones of the Bushveld Complex, South-Africa. Lithos 125: 537–552

Griffin WL, Begg GC, O'Reilly SY (2013) Continental-root control on the genesis of magmatic ore deposits. Nat Geosci 6:905–910

Hart SR, Dunn T (1993) Experimental cpx/melt partitioning of 24 trace elements. Contrib Mineral Petrol 113:1–8

Hauri EH, Wagner TP, Grove TL (1994) Experimental and natural partitioning of Th, U, Pb and other trace elements between garnet, clinopyroxene and basaltic melts. Chem Geol 117:149–166

Hill E, Wood BJ, Blundy JD (2000) The effect of Ca-Tschermaks component on trace element partitioning between clinopyroxene and silicate melt. Lithos 53:203–215

Hill E, Blundy JD, Wood BJ (2011) Clinopyroxene-melt trace element partitioning and the development of a predictive model for HFSE and Sc. Contrib Miner Petrol 161:423–438

Hou T, Zhang ZC, Encarnacion J, Santosh M, Sun YL (2013) The role of recycled oceanic crust in magmatism and metallogeny: Os–Sr–Nd isotopes, U–Pb geochronology and geochemistry of picritic dykes in the Panzhihua giant Fe-Ti oxide deposit, central Emeishan large igneous province, SW China. Contrib Miner Petrol 165:805–822

Holwell DA, Keays RR (2014) The Formation of Low-Volume, High-Tenor Magmatic PGE-Au Sulfide Mineralization in Closed Systems: Evidence from Precious and Base Metal Geochemistry of the Platinova Reef, Skaergaard Intrusion, East Greenland. Econ Geol 109:387–406

Howarth GH, Prevec SA (2013) Trace element, PGE, and Sr–Nd isotope geochemistry of the Panzhihua mafic layered intrusion, SW China: Constraints on ore-forming processes and evolution of parent magma at depth in a plumbing-system. Geochim Cosmochim Acta 120: 459–478

Hu AQ, Zhang GX, Chen YB (2006) Isotope Geochronology and Geochemistry for Major Geological Events of Continental Crustal Evolution of Xinjiang, China. Geological Publishing House, Beijing, pp 427 (in Chinese)

Huang H, Zhang ZC, Kusky T, Santosh M, Zhang S, Zhang DY, Liu JL, Zhao ZD (2012) Continental vertical growth in the transitional zone between South Tianshan and Tarim, western Xinjiang, NW China: Insight from the Permian Halajun A1-type granitic magmatism. Lithos 155:49–66

Jia CZ (1997) Tectonic characteristics and oil-gas in the Tarim Basin, China. Petroleum Industry Press, Beijing, pp 85–92, in Chinese

Jiang CY, Zhang PB, Lu DR, Bai KY (2004a) Petrogenesis and magma source of the ultramafic rocks at Wajilitag region, western Tarim Plate in Xinjiang. Acta Petrol Sin 20:1433–1444 (in Chinese with English abstract)

Jiang CY, Jia CZ, Li LC, Zhang PB, Lu DR, Bai KY (2004b) Source of the Fe-enriched-type high-Mg magma in Mazhartag region, Xinjiang. Acta Geol Sin 78:770–780 (in Chinese)

Jiang CY, Cheng SL, Ye SF, Xia MZ, Jiang HB, Dai YC (2006) Lithogeochemistry and petrogenesis of Zhongposhanbei mafic rock body, at Beishan region, Xinjiang. Acta Petrol Sin 22:115–126 (in Chinese with English abstract)

Kamenetsky VS, Chung SL, Kamenetsky MB, Kuzmin DV (2012) Picrites from the Emeishan large igneous province, SW China: a compositional continuum in primitive magmas and their respective mantle sources. J Petrol 53:2095–2113

Keays RR (1995) The role of komatiitic and picritic magmatism and S-saturation in the formation of ore deposits. Lithos 34:1–18

Kelemen PB, Hanghoj K, Greene AR (2004) One view of the geochemistry of subduction-related magmatic arcs, with an emphasis on primitive andesite and lower crust. In: Rudnick RL (ed) Treatise on geochemistry, vol 3. Elsevier, Amsterdam, pp 593–659

Lambert DD, Walker RJ, Morgan JW, Shirey SB, Carlson RW, Zientek ML, Lipin BR, Koski MS, Cooper RL (1994) Re–Os and Sm–Nd isotope geochemistry of the Stillwater Complex, Montana: Implications for the petrogenesis of the J-M Reef. J Petrol 35: 1717–1753

Lambert DD, Frick LR, Foster JG, Li CS, Naldrett AJ (2000) Re–Os isotopic systematics of the Voisey's Bay Ni-Cu-Co magmatic sulfide system. Canada: II. Implications for parental magma chemistry, ore genesis, and metal redistribution. Econ Geol 95:867–888

Li CS, Ripley EM (2005) Empirical equations to predict the sulfur content of mafic magmas at sulfide saturation and applications to magmatic sulfide deposits. Miner Deposita 40:218–230

Li CS, Ripley EM (2009) Sulfur contents at sulfide-liquid or anhydrite saturation in silicate melts: empirical equations and example applications. Econ Geol 104:405–412

Li CS, Maier WD, de Waal SA (2001) Magmatic Ni-Cu versus PGE deposits: contrasting genetic controls and exploration implications. S Afr J Geol 104:309–318

Li YQ, Li ZL, Sun YL, Chen HL, Yang SF, Yu X (2010) PGE and geochemistry of Wajilitag ultramafic cryptoexplosive brecciated rocks from Tarim Basin: Implications for petrogenesis. Acta Petrol Sin 26:3307–3318 (in Chinese with English abstract)

Li ZL, Chen HL, Song B, Li YQ, Yang SF, Yu X (2011) Temporal evolution of the Permian large igneous province in Tarim Basin in northwestern China. J Asian Earth Sci 42:917–927

Li YQ, Li ZL, Chen HL, Yang SF, Yu X (2012a) Mineral characteristics and metallogenesis of the Wajilitag layered mafic–ultramafic intrusion and associated Fe-Ti-V oxide deposit in the Tarim large igneous province, northwest China. J Asian Earth Sci 49:161–174

Li YQ, Li ZL, Sun YL, Santosh M, Langmuir CH, Chen HL, Yang SF, Chen ZX, Yu X (2012b) Platinum-group elements and geochemical characteristics of the Permian continental flood basalts in the Tarim Basin, northwest China: implications for the evolution of the Tarim large igneous province. Chem Geol 328:278–289

Li CS, Tao Y, Qi L, Ripley EM (2012c) Controls on PGE fractionation in the Emeishan picrites and basalts: constraints from integrated lithophile–siderophile elements and Sr–Nd isotopes. Geochim Cosmochim Acta 90:12–32

Lightfoot PC, Keays RR, Evans-Lamswood D, Wheeler R (2012) S saturation history of Nain Plutonic Suite mafic intrusions: origin of theVoisey's Bay Ni-Cu-Co sulfide deposit, Labrador, Canada. Miner Deposita 47:23–50

Liu PP, Zhou MF, Wang CY, Xing CM, Gao JF (2014) Open magma chamber processes in the formation of the Permian Baima mafic-ultramafic layered intrusion, SW China. Lithos 184:194–208

Long XP, Yuan C, Sun M, Zhao GC, Xiao WJ, Wang YJ, Yang YH, Hu AQ (2010) Archean crustal evolution of the northern Tarim craton, NW China: Zircon U–Pb and Hf isotopic constraints. Precambrian Res 180:272–284

Lorand JP (1993) Comment on "Content and isotopic composition of sulphur in ultramafic xenoliths from central Asia" by Ionov DA, Hoefs J, Wedepohl KH, Wie-chert U. Discussion. Earth Planet Sci Lett 119:627–634

Lundstrom C, Shaw HF, Ryerson FJ, Williams Q, Gill J (1998) Crystal chemical control of clinopyroxene-melt partitioning in the Di-Ab-An system: Implications for elemental fractionations in the depleted mantle. Geochim Cosmochim Acta 62:2849–2862

Maier WD (2005) Platinum-group element (PGE) deposits and occurrences: mineralization styles, genetic concepts, and exploration criteria. J Afr Earth Sci 41:165–191

Maier WD, Groves DI (2011) Temporal and spatial controls on the formation of magmatic PGE and Ni-Cu deposits. Miner Deposita 46: 841–857

Maier WD, Barnes SJ, Gartz V, Andrews G (2003) Pt-Pd reefs in magnetitites of the Stella layered intrusion, South Africa: a world of new exploration opportunities for platinum group elements. Geology 31:885–888

Mao JW, Pirajno F, Zhang ZH, Chai FM, Wu H, Chen SP, Cheng LS, Yang JM, Zhang CQ (2008) A review of Cu-Ni sulphide deposits in the Chinese Tianshan and Altay orogens (Xinjiang Autonomous Region, NW China): Principal characteristics and ore-forming processes. J Asian Earth Sci 32:184–203

Mavrogenes JA, O'Neill HSC (1999) The relative effects of pressure, temperature and oxygen fugacity on the solubility of sulfide in mafic magmas. Geochim Cosmochim Acta 63:1173–1180

McDonough WF, Sun SS (1995) The composition of the Earth. Chem Geol 120:223–253

McKenzie D, O'Nions RK (1991) Partial melt distributions from inversion of rare earth element concentrations. J Petrol 32:1021–1091

Meisel T, Walker RJ, Irving AJ, Lorand JP (2001) Osmium isotopic compositions of mantle xenoliths: a global perspective. Geochim Cosmochim Acta 65:1311–1323

Mungall JE, Naldrett AJ (2008) Ore deposits of the platinum-group elements. Elements 4:253–258

Naldrett AJ (2004) Magmatic sulfide deposits: geology, geochemistry, and exploration. Heidelberg, Berlin, Springer Verlag, p 727

Naldrett AJ, Wilson A, Kinnaird J, Chunnett G (2009) PGE tenor and metal ratios within and below the Merensky Reef, Bushveld Complex: implications for its genesis. J Petrol 50:625–659

Naldrett AJ (2010) From the mantle to the bank: the life of a Ni-Cu-(PGE) sulfide deposit. S Afr J Geol 113:1–32

Pang KN, Zhou MF, Qi L, Shellnutt JG, Wang CY, Zhao DG (2010) Magmatic Fe-Ti-V oxide deposits in the Emeishan large igneous province, SW China. Lithos 119:123–136

Pirajno F, Mao JW, Zhang ZC, Zhang ZH, Chai FM (2008) The association of mafic-ultramafic intrusions and A-type magmatism in the Tianshan and Altay orogens, NW China: implications for geodynamic evolution and potential for the discovery of new ore deposits. J Asian Earth Sci 32:165–183

Pirajno F, Ernst RE, Borisenko AS, Fedoseev G, Naumov EA (2009) Intraplate magmatism in Central Asia and China and associated metallogeny. Ore Geol Rev 35:114–136

Poujol M, Anhaeusser CR, Armstrong RA (2002) Episodic granitoid emplacement in the Archaean Amalia–Kraaipan terrane, South Africa: confirmation from single zircon U–Pb geochronology. J Afr Earth Sci 35:147–161

Prendergast MD (2000) Layering and precious metals mineralization in the Rincón del Tigre Complex, Eastern Bolivia. Econ Geol 95:113–130

Qi L, Wang CY, Zhou MF (2008) Controls on the PGE distribution of Permian Emeishan alkaline and peralkaline volcanic rocks in Longzhoushan, Sichuan Province, SW China. Lithos 106:222–236

Qin KZ, Zhang LC, Xiao WJ (2003) Overview of major Au, Cu, Ni and Fe deposits and metallogenic evolution of the eastern Tianshan Mountains, Northwestern China. In: Mao JW, Goldfarb RJ, Seltrnan R, Wang DW, Xiao WJ and Hart C (ed), Tectonic Evolution and Metallogeny of the Chinese Altay and Tianshan (London), pp 227–249

Qin KZ, Su BX, Sakyi PA, Tang DM, Li XH, Sun H, Xiao QH, Liu PP (2011) SIMS zircon U–Pb geochronology and Sr–Nd isotopes of Ni–Cu-bearing mafic-ultramafic intrusions in Eastern Tianshan and Beishan in correlation with flood basalts in Tarim Basin (NW China): Constraints on a ca. 280 Ma mantle plume. Am J Sci 311:237–260

Ren MH, Sun YL, Wang CY, Sun SL (2016) Determination of platinum-group elements in geological samples by isotope dilution-inductively coupled plasma-mass spectrometry combined with sulfide fire assay preconcentration. Geostand Geoanal Res 40:67–83

Rollinson (1993) Using Geochemical Data: Evolution, Presentation, Interpretation. Harlow, Longman Scientific and Technical, pp 352

Rui XJ, He JR, Guo KY (2002) Mineral resources of Tarim Block. Geological Publishing House, Beijing, pp 56–157, in Chinese with English abstract

Sa JHS, Barnes SJ, Prichard HM, Fisher PC (2005) The distribution of base metals and platinum-group elements in magnetitite and its host rocks in the Rio Jacare intrusion, Northeastern Brazil. Econ Geol 100:333–348

Said N, Kerrich R, Groves DI (2010) Geochemical systematics of basalts of the Lower Basalt Unit, 2.7 Ga Kambalda Sequence, Yilgarn craton, Australia: plume impingement at a rifted craton margin. Lithos 115:82–100

Savard D, Barnes SJ, Meisel T (2010) Comparison between nickel-sulfur fire assay Te Co-precipitation and isotope dilution with high-pressure asher acid digestion for the determination of platinum-group elements, rhenium and gold. Geostand Geoanal Res 34:281–291

Schoenberg R, Nägler TF, Gnos E, Kramers JD, Kamber BS (2003) The source of the Great Dyke, Zimbabwe, and its tectonic significance: evidence from Re–Os isotopes. J Geol 111:565–578

Shirey SB, Walker RJ (1995) Carius tube digestion for low-blank rhenium-osmium analysis. Analyt Chem 67:2136–2141

Shirey SB, Walker RJ (1998) The Re–Os isotope system in cosmochemistry and high- temperature geochemistry. Annu Rev Earth Planet Sci 26:423–500

Su BX, Qin KZ, Sun H, Tang DM, Xiao QH, Cao MJ (2009) Petrological and mineralogical characteristics of Hongshishan mafic-ultramafic complex in Beishan area, Xinjiang: implications for assimilation and fractional crystallization. Acta Petrol Sin 25:873–887 (in Chinese with English abstract)

Su BX, Qin KZ, Sakyi PA, Li XH, Yang YH, Sun H, Tang DM, Liu PP, Xiao QH, Malaviarachchi SPK (2011) U–Pb ages and Hf–O isotopes of zircons from Late Paleozoic mafic-ultramafic units in the southern Central Asian Orogenic Belt: tectonic implications and evidence for an Early-Permian mantle plume. Gondwana Res 20:516–531

Sun SS, McDonough WF (1989) Chemical and isotopic systematics of oceanic basalts: implications for mantle composition and processes. In: Saunders AD, Norry MJ (ed), Magmatism in the Ocean Basins. Geol Soc Spec Publ 42:313–345

Sun H, Qin KZ, Li JX, Tang DM, Fan X, Xiao QH (2008) Constraints of mantle partial melting on PGE mineralization of mafic–ultramafic intrusions in the East Tianshan: case study on Tulaergen and Xiangshan Ni-Cu deposits. Acta Petrol Sin 24:1079–1068, in Chinese with English abstract

Sun Y, Xiao YF, Zhao XK, Qian YX, Xiao GW, Liu HQ (2009a) The zircon U–Pb age of mazhaertage alkalic complex in the Tarim Basin and its geologic significance. Acta Geol Sin 83:775–781 (in Chinese)

Sun YL, Chu ZY, Sun M, Xia XP (2009b) An improved Fe–Ni sulfide fire assay method for determination of Re, platinum group elements, and Os isotopic ratios by inductively coupled plasma- and negative thermal ionization-mass spectrometry. Appl Spectrosc 63:1232–1237

Sun T, Qian ZZ, Deng YF, Li CS, Song XY, Tang QY (2013) PGE and isotope (Hf–Sr–Nd–Pb) constraints on the origin of the Huangshandong magmatic Ni–Cu sulfide deposit in the Central Asian Orogenic Belt, NW China. Econ Geol 108:184–1864

Tang DM, Qin KZ, Sun H, Su BX, Xiao QH, Cheng SL, Li J (2009) Zircon U–Pb age and geochemical characteristics of Tianyu intrusion, East Tianshan: constraints on source and genesis of mafic-ultramafic intrusions in East Xinjiang. Acta Petrol Sin 25:817–831 (in Chinese with English abstract)

Tian W, Campbell IH, Allen CM, Guan P, Pan WQ, Chen MM, Yu HJ, Zhu WP (2010) The Tarim picrite-basalt-rhyolite suite, a Permian flood basalt from northwest China with contrasting rhyolites produced by fractional crystallization and anatexis. Contrib Mineral Petrol 160:407–425

Vogel DC, Keays RR (1997) The petrogenesis and platinum-group element geochemistry of the Newer Volcanic province, Victoria, Australia. Chem Geol 136:181–204

Walker RJ, Morgan JW, Hanski EJ, Smolkin V (1997) Re–Os systematics of Early Proterozoic ferropicrites, Pechenga Complex, NW Russia: evidence for ancient [187]Os-enriched plumes. Geochim Cosmochim Acta 61:3145–3160

Wang CY, Zhou MF, Qi L (2010) Origin of extremely PGE-rich mafic magma system: an example from the Jinbaoshan ultramafic sill, Emeishan large igneous province, SW China. Lithos 119:147–161

Wang CY, Zhou MF, Yang SH, Qi L, Sun YL (2014) Geochemistry of the Abulangdang intrusion: cumulates of high-Ti picritic magmas in the Emeishan large igneous province, SW China. Chem Geol 378–379: 24–39

Wei X, Xu YG (2011) Petrogenesis of Xiaohaizi syenite complex from Bachu area, Tarim. Acta Petrol Sin 27:2984–3004 (in Chinese with English abstract)

Wei X, Xu YG, Feng YX, Zhao JX (2014a) Plume-lithosphere interaction in the generation of the Tarim large igneous province, NW China: geochronological and geochemical constraints. Am J Sci 314:314–356

Wei X, Xu YG, Zhang CL, Zhao JX, Feng YX (2014b) Petrology and Sr–Nd Isotopic Disequilibrium of the Xiaohaizi Intrusion, NW China: Genesis of Layered Intrusions in the Tarim Large Igneous Province. J Petrol 55:2567–2598

Widom E, Shirey SB (1996) Os isotope systematics in the Azores: implications for mantle plume sources. Earth Planet Sci Lett 142:451–465

Wilson AH, Prendergast MD (2001) Platinum-group element mineralisation in the Great Dyke Zimbabwe and its relationship to magma evolution and magma chamber structure. S Afr J Geol 104: 318–342

XBGR (Xinjiang Bureau of Geology and Resources) (1993) Regional Geology of the Xinjiang Uygur Autonomous Region. Geological Publishing House, Beijing, pp 1–48, in Chinese

Xiao F, Wang MF, Jiang CL, Yang WS (2013) Platinum group elements geochemistry and its implications for the Xiangshan Cu-Ni sulfide deposit, East Tianshan, China. Geological Science and Technology Information 32:125–138

Xu YG, Chung SL, Jahn BM, Wu GY (2001) Petrologic and geochemical constraints on the petrogenesis of Permian-Triassic Emeishan flood basalts in southwestern China. Lithos 58:145–168

Xu YG, Wei X, Luo ZY, Liu HQ, Cao J (2014) The Early Permian Tarim Large Igneous Province: main characteristics and a plume incubation model. Lithos 204:20–35

Yang SF, Chen HL, Dong CW, Jia CZ, Wang ZG (1996) The discovery of Permian syenite inside Tarim basin and its geodynamic significance. Geochemica 25:121–128 (in Chinese with English abstract)

Yang SF, Li ZL, Chen HL, Xiao WJ, Yu X, Lin XB, Shi XG (2006) Discovery of a Permian quartz syenitic porphyritic dyke from the Tarim Basin and its tectonic implications. Acta Petrol Sin 22:1405–1412 (in Chinese with English abstract)

Yang SF, Li ZL, Chen HL, Santosh M, Dong CW, Yu X (2007a) Permian bimodal dyke of Tarim Basin, NW China: geochemical characteristics and tectonic implications. Gondwana Res 12:113–120

Yang SF, Yu X, Chen HL, Li ZL, Wang QH, Luo JC (2007b) Geochemical characteristics and petrogenesis of Permian Xiaohaizi ultrabasic dyke in Bachu area, Tarim Basin. Acta Petrol Sin 23:1087–1096 (in Chinese with English abstract)

Yang SF, Chen HL, Li ZL, Li YQ, Yu X, Li DX, Meng LF (2013) Early Permian Tarim Large Igneous Province in northwest China. Sci China Ser D Earth Sci 56:2015–2026

Yang SH, Zhou MF, Lightfoot PC, Xu JF, Wang CY, Jiang CY, Qu WJ (2014) Re–Os isotope and platinum-group element geochemistry of the Pobei Ni-Cu sulfide-bearing mafic-ultramafic complex in the northeastern part of the Tarim Craton. Miner Deposita 49:381–397

Yu X (2009) Magma evolution and deep geological processes of early Permian Tarim large igneous province. Ph.D thesis, Zhejiang University, China (in Chinese with English abstract)

Yu X, Yang SF, Chen HL, Chen ZQ, Li ZL, Batt GE, Li YQ (2011) Permian flood basalts from the Tarim Basin, Northwest China: SHRIMP zircon U–Pb dating and geochemical characteristics. Gondwana Res 20:485–497

Yuan F, Zhou TF, Zhang DY, Jowitt SM, Keays RR, Liu S, Fan Y (2012) Siderophile and chalcophile metal variations in basalts: implications for the sulfide saturation history and Ni-Cu-PGE mineralization potential of the Tarim continental flood basalt province, Xinjiang Province, China. Ore Geol Rev 45:5–15

Zhang CL, Zou HB (2013a) Permian A-type granites in Tarim and western part of Central Asian Orogenic Belt (CAOB): Genetically related to a common Permian mantle plume ? Lithos 172–173:47–60

Zhang CL, Zou HB (2013b) Comparison between the Permian mafic dykes in Tarim and the western part of Central Asian Orogenic Belt (CAOB), NW China: implications for two mantle domains of the Permian Tarim Large Igneous Province. Lithos 174:15–27

Zhang CL, Li XH, Li ZX, Ye HM, Li CN (2008a) A Permian layered intrusive complex in the Western Tarim Block, Northwestern China: Product of a ca. 275-Ma mantle plume? J Geol 116:269–287

Zhang M, O'Reilly SY, Wang KL, Hronsky J, Griffin WL (2008b) Flood basalts and metallogeny: the lithospheric mantle connection. Earth Sci Rev 86:145–174

Zhang CL, Xu YG, Li ZX, Wang HY, Ye HM (2010a) Diverse Permian magmatism in the Tarim Block, NW China: genetically linked to the Permian Tarim mantle plume? Lithos 119:537–552

Zhang CL, Li ZX, Li XH, Xu YG, Zhou G, Ye HM (2010b) A Permian large igneous province in Tarim and Central Asian orogenic belt, NW China: results of a ca. 275 Ma mantle plume? Geol Soc Am Bull 122:2020–2040

Zhang CL, Zhou G, Wang HY, Dong YG, Ding RF (2010c) A review on two types of mantle domains of the Permian large igneous province in Tarim and the western section of Central Asian orogenic belt. Geol Bull Chin 29:779–794

Zhang CL, Li HK, Santosh M, Li ZX, Zou HB, Wang HY, Ye HM (2012) Precambrian evolution and cratonization of the Tarim Block, NW China: Petrology, geochemistry, Nd-isotopes and U–Pb zircon geochronology from Archean gabbro-TTG- potassic granite suite and Paleoproterozoic metamorphic belt. J Asia Ear Sci 47:5–20

Zhang CL, Zou HB, Li HK, Wang HY (2013a) Tectonic framework and evolution of the Tarim Block in NW China. Gondwana Res 23: 1306–1315

Zhang CJ, Wang HJ, Shi GH (2013b) The geological features and mine prospecting significance of Puchang ilmenite mine in Atushi, Xinjiang. Xinjiang Geol 31:29–33 (in Chinese with English abstract)

Zhang XQ, Song XY, Chen LM, Yu SY, Xie W, Deng YF, Zhang JF, Gui SG (2013c) Chalcophile element geochemistry of the Baima layered intrusion, Emeishan Large Igneous Province, SW China: implications for sulfur saturation history and genetic relationship with high-Ti basalts. Contrib Mineral Petrol 166:193–209

Zhang DY, Zhang ZC, Huang H, Encarnación J, Zhou NW, Ding XX (2014) Platinum-group elemental and Re–Os isotopic geochemistry of the Wajilitag and Puchang Fe–Ti–V oxide deposits, northwestern Tarim Large Igneous Province. Ore Geol Rev 57:589–601

Zhong H, Zhou XH, Zhou MF, Sun M, Liu BG (2002) Platinum-group element geochemistry of the Hongge Fe-V-Ti deposit in the Pan-Xi area, southwestern China. Mineral Deposita 37:22–239

Zhong H, Qi L, Hu RZ, Zhou MF, Gou TZ, Zhu WG, Liu BG, Chu ZY (2011) Rhenium–osmium isotope and platinum-group elements in the Xinjie layered intrusion, SW China: Implications for source mantle composition, mantle evolution, PGE fractionation and mineralization. Geochim Cosmochim Acta 75:1621–1641

Zhou MF, Lesher CM, Yang ZX, Li JW, Sun M (2004) Geochemistry and petrogenesis of 270 Ma Ni-Cu-(PGE) sulfide-bearing mafic intrusions in the Huangshan district, Eastern Xinjiang, Northwest China: Implications for the tectonic evolution of the Central Asian orogenic belt. Chem Geol 209:233–257

Zhou LX, Hu SL, Wang LG, Li YJ, Huang ZB, Zhu HY, Zhao Y, Liu YL (2010) The age of Piqiang gabbroid, NW margin of Tarim Basin, NW China. Chin J Geol 45:1057–1065

Zhou MF, Robinson PT, Lesher CM, Keays RR, Zhang CJ, Malpas J (2005) Geochemistry, petrogenesis and metallogenesis of the

Panzhihua gabbroic layered intrusion and associated Fe-Ti-V oxide deposits, Sichuan province, SW China. J Petrol 46:2253–2280

Zhou MF, Arndt NT, Malpas J, Wang CY, Kennedy AK (2008) Two magma series and associated ore deposit types in the Permian Emeishan Large Igneous Province, SW China. Lithos 103:352–368

Zhou MF, Zhao JH, Jiang CY, Gao JF, Wang W, Yang SH (2009) OIB-like, heterogeneous mantle sources of Permian basaltic magmatism in the western Tarim Basin, NW China: Implications for a possible Permian large igneous province. Lithos 113:583–594

Zhu WB, Zheng BH, Shu LS, Ma DS, Wu HL, Li YX, Huang WT, Yu JJ (2011) Neoproterozoic tectonic evolution of the Precambrian Aksu blueschist terrane, north western Tarim, China: Insights from LA–ICP–MS zircon U–Pb ages and geochemical data. Precambrian Res 185:215–230

Zindler A, Hart S (1986) Chemical geodynamics. Annu Rev Earth Planet Sci 14:493–571

Zou SY, Li ZL, Song B, Ernst RE, Li YQ, Ren ZY, Yang SF, Chen HL, Xu YG, Song XY (2014) Zircon U–Pb dating, geochemistry and Sr–Nd–Pb–Hf isotopes of the Wajilitag alkali mafic dikes, and associated diorite and syenitic rocks: implications for magmatic evolution of the Tarim Large Igneous Province. Lithos 212–215:428–442